SLAC-PUB-789
UCRL-20223
December 1970

π^-p ELASTIC SCATTERING IN THE CMS ENERGY RANGE 1400-2000 MEV*

A. D. Brody,** R. J. Cashmore, A. Kernan,***
D.W.G.S. Leith, B. S. Levi, B. C. Shen***

Stanford Linear Accelerator Center
Stanford University, Stanford, California 94305

J. P. Berge,† D. J. Herndon, R. Longacre, L. R. Price,††
A. H. Rosenfeld, P. Soding†††

Lawrence Radiation Laboratory
University of California, Berkeley, California 94720

ABSTRACT

Total and differential cross sections for π^-p elastic scattering are presented at 35 energies between 1400 and 2000 MeV.

(Submitted to Phys. Rev.)

---

*Work supported by the U. S. Atomic Energy Commission.

**Present address is CERN, Geneva, Switzerland.

***Present address is University of California, Riverside, California.

†Present address is Department of Nuclear Physics, Oxford University, Oxford, England.

††Present address is University of California, Irvine, California.

†††Present address is DESY, Hamburg, West Germany.

I. INTRODUCTION

In recent years a large amount of data has been accumulated on the elastic and charge exchange channels of πN scattering. Several extensive phase shift analyses[1-7] performed on this data have uncovered much of the complicated resonance structure up to energies of 2000 MeV. The data and phase shift results have been summarized by a number of authors.[8-11] Resonance parameters from some of the recent analyses are listed in Table I.[12] Despite good qualitative agreements, quantitative discrepancies still exist among the various solutions. These discrepancies exist in part because of the multidimensional parameter space explored and the different methods used, from fluctuations between different experimental measurements, and finally from the fact that the elastic data used is fairly insensitive to partial waves of low elasticity. Thus, the motivation for the present experiment was to fill the need for direct measurement of the inelastic channels. The systematic and rather complete set of measurements of the elastic channel, described in this paper, came as a by-product of this inelastic study.

We present below the first part of the results of a study of elastic and inelastic $\pi^- p$ scattering at 35 momenta between 550 and 1600 MeV/c. Figure 1 illustrates the scope of the experiment. At each momentum the following reactions were measured:

$$\pi^- p \rightarrow \pi^- p \tag{1}$$

$$\rightarrow n\pi^+\pi^- \tag{2}$$

$$\rightarrow p\pi^-\pi^0 \tag{3}$$

$$\rightarrow \Lambda^0 K^0 \tag{4}$$

$$\rightarrow \Sigma^{0,-} K^{0,+} \tag{5}$$

This paper concerns only reaction (1). Reactions (2) and (3) are currently being studied both in terms of a quasi-two body final state and in terms of a three-body analysis. The results of these studies as well as the strange particle data will be presented in separate communications. Finally, we are extending the experiment to higher momenta, up to 2.25 BeV/c, as illustrated by the dotted lines in Fig. 1.

Organization of this paper is as follows:

Section IIA.	Experimental Details
IIB.	Film Measurement
III.	Data Analysis
IV.	Results
V.	Discussion

II.

A. Experimental Details

The experiment was performed using the 30-inch MURA HBC at the Argonne National Laboratory and the 72-inch Alvarez HBC at Berkeley. The Argonne exposure consists of ~ 500,000 pictures taken at 26 momenta between 550 and 865 MeV/c and between 1060 and 1600 MeV/c. The Berkeley exposure comprises about 200,000 pictures taken at 9 momenta between 925 and 1175 MeV/c. This latter film had been taken ten years previously, to study strange particle events about Λ, Σ threshold,[13] but had not been used to investigate the two-prong events.

The Argonne film was taken during three separate exposures in 1967. The beam was the "7^o" separated beam[14] of the ZGS. The higher momentum exposures used the mode shown in Fig. 2a and b. Here the first stage provided at slit 1 both a momentum focus in the horizontal plane and an image of the target in the vertical plane. The second stage provided a momentum focus at the final slit together with an image of the target in both planes. A simplified version of the beam, Fig. 2c, was used for the low momentum exposures. (i.e., $p_\pi < 1$ GeV/c.) The low energy pion flux was found to be much less than expected, and as a result it was not possible to obtain a useful beam below 580 MeV/c.

To produce an ideal shape (5" wide and 6" high) for the beam trajectory in the chamber further quadrupoles were used after the final slit. Since the image at the final slit had little vertical divergence, it was most effective to rotate the first quadrupole 45^o to couple optically the vertical and horizontal planes. The second quadrupole then increased the vertical divergence and decreased the horizontal divergence.

The high field of the 30-inch HBC and the low momentum of the beam made it necessary to raise the center of the chamber 7" above the center beam line and then to pitch the beam downwards into the fringe field of the bubble chamber magnet to obtain a good trajectory of the beam through the chamber. Finally, for momenta below 870 MeV/c it was further necessary to lower the HBC magnet current from 20,000 amps to 12,000 amps, to maintain this trajectory.

The proton beam of the ZGS gave a pulse of pions once every 2.9 seconds. For part of the exposure, the bubble chamber was triple pulsed during each beam spill, allowing a rate of nearly 1 picture per second.

The π^- beam used for the Berkeley exposure is sketched in Fig. 3. It has been previously described[15] for a momentum setting of 1030 MeV/c. The characteristics remain the same at the momenta used in the present experiment. In particular the beam is characterized by good momentum resolution, the fractional momentum bite $\Delta p/p$ being on the order of $\pm .5\%$.

All beam interactions within the volume 34 cm wide, 122 cm long and 9 cm deep were accepted from the 72 inch chamber, while for the 30-inch chamber, the fiducial volume was defined as 58 cm long, 58 cm wide and 16 cm deep.

The coordinate system for both chambers is defined with the camera axis as the z-axis and the beam coincident with the y-axis. In the Alvarez chamber, the camera axis is tilted $7\frac{1}{2}^{o}$ with respect to the vertical axis.

The magnetic fields of both chambers were determined by extrapolating from previously measured field maps. These existed for the 72-inch chamber at magnet current settings of 2400A, 3500A and 4600A. The measured values of the B_z at these currents were fitted with a 27-term polynomial expansion[16] and the horizontal components were calculated to satisfy Maxwell's equations to third power in xy. These coefficients were scaled where necessary to the settings of 3102A, 3690A, 2600A and 4600A used in the present experiment. The value of B_z at the center of the chamber was determined by looking at K^o decays ($K^o \rightarrow \pi^+ + \pi^-$) and elastic scatters. We required that the distribution in the unfit invariant mass of the π^+ and π^- agreed with the accepted K^o mass. We also required that the distributions in measured and fitted values of the momenta of each track in the 4C (elastic scatter) events agreed. We found that both of these criteria were simultaneously satisfied in most regions of our film rather easily.

The same procedure was adopted to determine the field of the 30-inch chamber. It was necessary to scale from the field map measured at 20,000A down to 12,000A. Two precautions were taken here. The field measurement at 20,000A agreed with the design calculations to within 1%. Furthermore the field shape was predicted to remain the same at lower current settings. As an additional check, the film taken at 853 MeV/c was divided between the two values of the field. The elastic scatters from the two fields were compared and no discernible differences were detected.

Table II summarizes the currents and central values of the fields used.

The optical constants required by the fitting programs were determined by making a 12 parameter least squares fit of measured fiducials to their known positions, using the program WEASEL. For the 72-inch HBC, 13 fiducials were measured, with many sets of measurements being obtained throughout the entire exposure. Several sets of measurements were averaged whenever appropriate with the program MONKEY. Each set of constants was checked by comparing measured quantities with corresponding fitted quantities of 4C elastic scattering events in all parts of the chamber. Although there was poor agreement at the edges of the chamber, satisfactory results were obtained within the fiducial volume. The pull distributions in Fig. 4d reflect the quality of spatial reconstruction.

The same procedure was used to determine the optical constants for the 30-inch MURA HBC. However, the reconstruction was slightly less satisfactory, because there were not enough visible fiducials to enable determination of the high order distortion parameters. The pull distributions are given in Fig. 4a - c.

B. Measurement

The bubble chamber film was scanned at SLAC and an LRL Spiral Reader used to measure the events. The scanners at SLAC recorded all two-prong events. Events in which the beam track disappeared for more than a projected length of 3mm before the vertex were classified as 0-prong, 1-vee events. Events were rejected if obscured in any way or if the beam track was less than 3 cm long. No bias is introduced by these rejects. Events in which both outgoing tracks were less than 1 cm were also rejected, introducing a loss of reactions with short protons. Such events correspond to CMS scattering angles which are not included in our results and analysis (see Section IV). However, a further bias is expected due to loss of short, dipping protons, and correction for this bias will be discussed in Section III.

The scanning efficiency was evaluated by rescanning approximately 20 percent of the Argonne film and 10 percent of the Berkeley film. The master lists from the first and second scans were then compared by the computer program CONFLICT, which lists all discrepancies. These discrepancies were examined again on the scan table to determine whether they were valid events. Following this procedure, the combined scan efficiency was found to be 97 percent.

The film was measured on an LRL Spiral Reader,[17] a semi-automatic film digitizing machine. The reader digitizations are connected into tracks by a FORTRAN filter program POOH.[18] With this program it is difficult to fit steeply dipping tracks, and the loss of such tracks constituted a bias which will be examined in the next section.

III. DATA ANALYSIS

The measured two-prong events are processed by the SIOUX-ARROW system programs. SIOUX consists of a three-view geometry program for spatial reconstruction and a fitting program which tries, in this experiment, each of the following hypotheses:

$$\pi^- p \to \pi^- p \tag{1}$$

$$\to n\pi^+\pi^- \tag{2}$$

$$\to p\pi^-\pi^0 \tag{3}$$

Since the 4C elastic hypothesis is more highly constrained than the 1C inelastic hypotheses, there is little contamination of these elastic events. Contamination is further reduced by the requirement that the ionization measured by the Spiral Reader be consistent with the fitted track momentum. The clean separation of the final sample 4C events is illustrated in Fig. 5, where we plot the square of the missing mass in the reaction:

$$\pi^- p \to \pi^- p \ \text{mm} \ .$$

This histogram is sharply peaked at zero, with a slight pull to the negative side, as expected in plots of this type.[19]

The center-of-mass energies are determined for each region of film from the fitted distributions of the 4C elastic events. Sample distributions are shown in Fig. 6. The beam has a low energy tail. In determining the mean value of the c.m. energy cutoffs were applied to the data. These cutoffs are given in Table V.

Because of the high momentum resolution of the Berkeley beam, the technique of "beam averaging" was used in processing this film. The momentum for a given event was a weighted average of 'beam average' and measured momenta, calculated from the expression:

$$p = \frac{p_{meas}/(\Delta p_{meas})^2 + p_{B.A.}/(\Delta p_{B.A.})^2}{1/(\Delta p_{meas})^2 + 1/(\Delta p_{B.A.})^2}$$

In order to determine the beam average momentum and its associated error, the following procedure was used. All events were processed through SIOUX without beam averaging. Those events fitting the 4C elastic scattering hypothesis with a $\chi^2 \leq 10$ were used to determine the average value of the beam momentum, $p_{B.A.}$, and its error, $\Delta p_{B.A.}$.

The efficiency for passing events through the measuring process and the filtering program was found to be 97 percent after the first measurement of the 72-inch HBC film. We made a repeat measurement of about 17,000 events and found the combined efficiency then to be 99 percent. All of the 30-inch HBC film was measured twice except for 43% which had unambiguous fits on the first measurement. The combined efficiency after the second measurement for all events in the 30-inch chamber was 93 percent. Those events which failed twice were examined on the scan table, and no evidence for topological bias was found apart from the bias against short protons mentioned previously. The number of events of each reaction type (1), (2) or (3) which were processed are given in Fig. 7 and in Table III.

Figure 8 shows the χ^2 distributions from our experiment. As usual in hydrogen bubble chamber experiments, the observed and theoretical chi-squared distributions agree satisfactorily provided that the theoretical χ^2 is scaled up by a factor. This 'scale' factor is indicated in Fig. 8. Elastic events with $\chi^2 < 25$ were used in the subsequent analysis. To test the sensitivity to the χ^2

cut-off, the Legendre polynomial coefficients describing the angular distributions were computed for those events with $\chi^2 \leq 25$, and for the subsample of events with $\chi^2 \leq 10$. The values of the coefficients were unchanged within their errors.

The data were corrected for loss of events in which the scattering plane lies close to the camera axis. If the angle α is defined as the angle between the normal to the scattering plane and the camera axis, then a depletion of events is expected at 90° for forward pion production angles, where the protons have a small range. However, the data show this expected loss not only in the forward regions but also in the middle and backward regions. This latter loss of events is due to the previously mentioned bias of the POOH filter program against steeply dipping tracks. Typical azimuthal distributions are shown in Fig. 9 for the forward, middle and backward production regions. The bias is strongest in the forward regions. Corrections for these biases were made separately by regions of production angle and energy and are listed in Table IV.

IV. RESULTS

In this section we present the results of our measurement of the $\pi^- p$ elastic scattering cross sections. In determining the angular distributions the c.m. energy cutoffs of Table V were used. Our data was normalized to counter experiment results in the range of scattering angles ($-0.8 \leq \cos\theta < 0.7$), where the experimental biases are not a serious problem for either counters or HBC. Specifically we have used the data of Duke et al.,[20] Helland et al.,[21] and Ogden et al.[22] It should be noted that this normalization region contributes only 20-30% of the total elastic cross section, and that it varies slowly as a function of energy throughout the region investigated (see Fig. 10). Thus, our measurement of the total cross section, and of the sharply varying energy dependencies is only weakly dependent on the fact that we have normalized to the counter work.

The elastic scattering angular distributions are presented in Fig. 11. The data is available in tabular form elsewhere.[23] The distributions extend up to $\cos\theta = .90$ below 1647 MeV and up to $\cos\theta = .95$ at higher energies. At more forward angles the recoiling proton has nearly zero range.

The smooth curves superposed on the data in Fig. 11 represent the best fit to a series expansion in Legendre polynomials, where

$$d\sigma/d\Omega = \sum_n A_n P_n (\cos\theta) \quad .$$

A fit to order n = 5 was sufficient below 1674 MeV, and to order n = 6 at higher energies. Table V lists the Legendre coefficients A_n for each energy, along with the χ^2 and confidence level describing the fit to the data. These coefficients are plotted in Fig. 12 along with those of other experiments.[20,22] The agreement is good.

The total elastic cross section was determined from the Legendre fit to the data using the relation:

$$\sigma_{el} = 4\pi A_0 \quad .$$

The elastic cross section is shown in Fig. 10 compared to the cross sections of the counter experiments.[20,21,22]

The forward cross section may be extrapolated from the Legendre coefficients according to

$$d\sigma/d\Omega\,(\theta=0) = \sum_n A_n \quad .$$

The forward elastic cross sections thus determined are the data points in Fig. 13. The smooth curve represents the forward cross section predicted by Carter.[24] The real part of the forward scattering amplitude was calculated from partial wave dispersion relations, while the imaginary part was obtained from the optical theorem using the recent precision total cross section measurements of Carter *et al.*[25] The curve shows a marked shift toward the low energy side of the third resonance peak. This shift reflects the shift of the data of Carter *et al.* compared to other experiments,[26, 27, 28, 29] as seen in Fig. 14.

The behavior of the Legendre coefficients reflects qualitatively the resonance structure. The fact that all coefficients up to and including A_5 show a strong peak near 1690 MeV indicates the presence of D_5 and F_5 resonances. Furthermore, the absence of any rapid variation or change of sign of A_5 implies that the D_5 and F_5 have a constant phase difference near the resonance peak.

The presence of a D_3 resonance is signaled by the bump in A_2 near 1520 MeV. The similar bump in A_1 can be attributed to interference of the D_3 with a P_1. The sign change in A_3 reflects interference of the D_3 with the P_3 resonance. (They are more than 90^o out of phase here.) Finally the fact that A_4 is consistent with zero implies zero interference between D_3 and D_5, (i.e., these waves must be about 90^o out of phase).

VI. DISCUSSION

While the Legendre coefficients indicate qualitatively the behavior of the dominant partial waves, more precise quantitative information is obtained from phase shift analyses. The dynamics of the interaction of a pion with a nucleon are contained in the partial wave amplitudes $T_\ell^\pm$ $J=\ell\pm\frac{1}{2}$. It is the behavior of these amplitudes which a phase shift analysis seeks to discover. The first step is thus to select some parameterization for these amplitudes. The T-matrix elements are related to the center-of-mass scattering amplitude through the following relations[30]

$$M = f(\theta) + g(\theta)\, \sigma \cdot n$$

where

$$f(\theta) = \frac{1}{\kappa} \sum_{\ell} \left\{ (\ell + 1)\, T_{\ell}^{+} + \ell T_{\ell}^{-} \right\} P_{\ell}(\cos\theta)$$

and

$$g(\theta) = \frac{i}{\kappa} \sum_{\ell} \left(T_{\ell}^{+} - T_{\ell}^{-} \right) P_{\ell}^{1}(\cos\theta)$$

$f(\theta)$ and $g(\theta)$ are the spin non-flip and spin-flip scattering amplitudes.

The differential cross section and polarization are then given by:

$$\frac{d\sigma}{d\Omega} = |M|^2 = |f|^2 + |g|^2$$

$$I\, \vec{P} = 2\, \mathrm{Re}(f^* g)\ \ \hat{n},$$

where

$$\hat{n} = \vec{\kappa}_i \times \vec{\kappa}_f / |\vec{\kappa}_i \times \vec{\kappa}_f|$$

The cross sections and polarizations predicted by the given parameters are compared with the experimental data and the parameters adjusted until a good fit is obtained. At the same time the parameters may be constrained by theoretical input. For example, all phase shift analyses require the parameters to satisfy some form of unitarity.

There are two main types of phase shift analysis — energy independent and energy dependent. Examples of the former are Saclay,[1] Berkeley[6] and the CERN[7] analysis, while Roper,[4] Chilton[2] and Glasgow[31] are examples of the latter type of analysis. The different methods are reviewed and compared elsewhere.[32]

In Fig. 15-18 our elastic cross section, and the differential cross section at six typical energies (shown by arrows in Fig. 15, 17) are compared to the predictions of the various phase shift analysis. In Fig. 15 the CERN solutions are shown. The comparison of CERN-Theoretical with the data has already been dealt with extensively in the literature,[33] while CERN-Experimental is seen to represent the data well, both in the cross section and the differential cross section (Fig. 16). In Fig. 17-18 the predictions of the Saclay, Berkeley and Glasgow work is shown to represent the data fairly well.

VI. CONCLUSION

The new elastic scattering data presented here confirms the general behavior shown by previous experiments. Because this experiment spans a wide energy region in a systematic way, it offers useful information for phenomenological analysis of πN scattering.

ACKNOWLEDGEMENTS

We wish to thank F. S. Crawford Jr., and J. A. Anderson for lending the LRL HBC film and helping to make that part of the experiment possible. We also wish to thank the LRL Spiral Reader crew and especially G. R. Lynch and L. J. Lloyd for their help and assistance in measuring the film, and the SLAC CDA staff for their scanning effort. Finally, we wish to acknowledge the valuable assistance at the early stage of the experiment of A. Minten and R. Diebold.

REFERENCES

1. P. Bareyre, C. Bricman, A. V. Stirling and G. Villet, Phys. Letters 18, 342 (1965); P. Bareyre, C. Bricman and G. Villet, Phys. Rev. 165, 1730 (1968).
2. B. H. Bransden, P. J. O'Donnell and R. G. Moorhouse, Phys. Letters 11, 339 (1964); Phys. Rev. 139B, 1566 (1965); Proc. Roy. Soc. (London) A289, 538 (1966); Phys. Letters 19, 420 (1965).
3. P. Auvil, A. Donnachie, A. T. Lea, and C. Lovelace, Phys. Letters 12, 76 (1964); 19, 148 (1965).
4. L. D. Roper, Phys. Rev. Letters 12, 340 (1964); L. D. Roper, R. M. Wright, and B. T. Feld, Phys. Rev. 138B, 190 (1965); L. D. Roper and R. M. Wright, Phys. Rev. 138B, 921 (1965).
5. R. J. Cence, Phys. Letters 20, 306 (1966).
6. C. H. Johnson, UCRL-17683 (1967).
7. A. Donnachie, R. G. Kirsopp, and C. Lovelace, Phys. Letters 26B, 161 (1968); C. Lovelace, Proceedings of the 1967 Heidelberg Conference (North Holland Publishing Co., Amsterdam, 1967); p. 79; H. Filthuth, ed., C. Lovelace, Invited paper at the Conference on πN Scattering, Irvine (1967); CERN Preprint TH-839 (1967).
8. R. G. Moorhouse, Ann. Rev. Nucl. Sci. 19, 301 (1969).
9. D. Herndon, A. Barbaro-Galtieri, A. H. Rosenfeld, UCRL-20030 πN, (1970); unpublished.
10. G. Giacomelli, P. Pini, S. Stagni, CERN/HERA 69-1.
11. G. L. Shaw, D. Y. Wang, N. Y. Wiley, Proceedings of the Pion-Nuclear Scattering Conference, Irvine, California (1967).

12. The contents of this table are taken from Particle Data Group: Phys. Letters 33B, 1 (1970). The various phase shift analyses are identified as

(1) P. Bareyre, C. Bricman and G. Villet, Phys. Rev. 165, 1730 (1968)

(2) P. Bareyre, C. Bricman and G. Villet, Phys. Rev. 165, 1730 (1968)

(3) Clarborne H. Johnson, Jr., Report No. UCRL-17683, Lawrence Radiation Laboratory (1967)

(4) A. Donnachie, R. G. Kirsopp and C. Lovelace, Phys. Rev. Letters 26B, 161 (1968)

(5) A. Donnachie, R. G. Kirsopp and C. Lovelace, Phys. Rev. Letters 26B, 161 (1968)

(6) R. G. Kirsopp, Ph.D. Thesis (unpublished)

(7) A. T. Davies, N.P. B21, 359 (1970).

(8) A. T. Davies, N.P. B21, 359 (1970).

(9) A. T. Lea, G. C. Oades, D. L. Ward, I. M. Cowan, W. M. Gibson, R. S. Gilmore, J. Malos, V. J. Smith, M.A.R. Kemp, Report No. RPP/H/57, Rutherford Laboratory (unpublished)

For a thorough discussion of each solution, we refer the reader to the original papers and the review articles.

13. F. S. Crawford, Proceedings of the International Conference on High Energy Physics at CERN (1962), p. 270; J. A. Anderson, UCRL 10838 (1963); J. Anderson, F. S. Crawford, Jr., and J. C. Doyle, Phys. Rev. 152, 1139 (1967); J. C. Doyle, F. S. Crawford, Jr., and J. A. Anderson, Phys. Rev. 165, 1483 (1968); J. C. Coyle, UCRL-18139 (1969).

14. T.H. Fields, E.L. Goldwasser, and U. E. Kruse, "Design for a 6 BeV/c separate K^- beam," A.N.L. Internal Report No. THF/ELG/UEK-1, (October 3, 1961, unpublished).

15. S. Wolf, N. Schmitz, L. Lloyd, W. Laskar, F. Crawford, Jr., J. Button, J. Anderson and G. Alexander, Rev. Mod. Phys. 33, 439 (1961).

16. SLAC physics note, APE Data Processing Note No. 1.

17. J. Lynch, Report No. UCRL-17238 (1967).

18. J. Burkhard, "Programming for flying spot devices," Proceedings of a Conference on Flying Spot Devices at Columbia (October 1965).

19. Basically this shift is due to the fact that E and p are correlated through the measured parameters. The correlation is such that $m^2 = E^2 - p^2$ is shifted to more negative values. This shift can be about as large as δm^2, especially for $m^2 = 0$. See "Missing mass calculations," S. Wojcicki and F. Solmitz, Alvarez Group Memo No. 367 (unpublished).

20. P. J. Duke, D. P. Jones, M.A.R. Kemp, P.G. Murphy, J. D. Prentice, J. J. Thresher, Phys. Rev. 149, 1077 (1966).

21. J. A. Helland, T. J. Devlin, D. E. Hagge, M. J. Longo, B. J. Moyer, and C. D. Wood, Phys. Rev. 134B, 1062 (1964); J. A. Helland, C. D. Wood, T. J. Devlin, D. E. Hagge, M. J. Longo, B. J. Moyer and V. Perez-Mendez, Phys. Rev. 134B, 1079 (1964).

22. D. M. Ogden, D. E. Hagge, J. A. Helland, M. Banner, J. F. Detoeuf, and J. Leiger, Phys. Rev. 137B, 115 (1965).

23. A. D. Brody, R. J. Cashmore, A. Kernan, D.W.G.S. Leith, B. S. Levi, B. C. Shen, J. P. Berge, D. J. Herndon, R. Longacre, L. R. Price, A. H. Rosenfeld, P. Soding, Report No. SLAC-PUB-789, Supplement 1.

24. A. A. Carter, "Real part of the pion-nucleon forward scattering amplitudes calculated from dispersion relations," Cavendish Laboratory Internal Report (unpublished).

25. A. A. Carter, F. K. Riley, R. J. Tapper, D. V. Bugg, R. S. Gilmore, K. M. Knight, D. C. Salter, G. H. Stafford, E.J.N. Wilson, J. D. Davies, J. D. Dowell, P. M. Hattersley, R. J. Homer and A. W. O'Dell, Phys. Rev. 168, 1457 (1968).

26. T. J. Devlin, B. J. Moyer and V. Perez-Mendez, Phys. Rev. 125, 690 (1962).

27. T. J. Devlin, J. Solomon and G. Bertsch, Phys. Rev. Letters 14, 1031 (1965).

28. J. C. Brisson, J. F. Detoeuf, P. Falk-Variant, L. Van Ressum, G. Valladas, and L.C.L. Yan, Nuovo Cimento 19, 210 (1961).

29. G. Bizard, J. Duchon, J. Sequinot, J. Yonnet, P. Bareyre, C. Bricman, G. Valladas and G. Villet, Nuovo Cimento 44, 999 (1966); M. Banner, P. Bareyre and C. Bricman (to be published in Nuovo Cimento); A. Stirling et al., cited by B. Ambland et al., Phys. Letters 10, 140 (1964).

30. M. L. Goldberger and K. M. Watson, Collision Theory (John Wiley and Sons, Inc., New York, 1964).

31. A. T. Davies, N.P. B21, 359 (1970).

32. A. D. Brody, R. J. Cashmore, A. Kernan, D.W.G.S. Leith, B. S. Levi, B. C. Shen, J. P. Berge, D. J. Herndon, R. Longacre, L. R. Price, A. H. Rosenfeld, P. Söding, Report No. SLAC-PUB-789, Supplement 2.

33. A. D. Brody, D.W.G.S. Leith, B. G. Levi, B. C. Shen, D. Herndon, R. Longacre, L. Price, A. H. Rosenfeld and P. Söding, Phys. Rev. Letters 22, 1401 (1969); A. Donnachie, C. Lovelace, Phys. Rev. D1, 956 (1970) (reply); A. D. Brody et al., Report No. SLAC-PUB-709 (reply).

TABLE CAPTIONS

I. S = 0 Baryon Resonances

II. Magnet Currents and Central Field Values

III. Events Processed at Each Energy

IV. Azimuthal Correction Factors and Errors

V. Legendre Polynomial Coefficients

$$\frac{d\sigma}{d\Omega} = \sum_n A_n P_n(\cos\theta)$$

TABLE I

S = 0 Baryon Resonances

I = 1/2 States

Phase Shift* Analysis	P_{11}(1470)			D_{13} (1520)			S_{11} (1535)			D_{13} (1700)			D_{15} (1670)			F_{15}(1688)		
	M	Γ	x	M	Γ	x	M	Γ	x	M	Γ	x	M	Γ	x	M	Γ	x
1	1470	255	0.68	1510	125	0.54	1535	155	-				1680	135	0.41	1690	110	0.64
2	1505	205	0.68	1515	110	0.54	1515	105	-	Possible			1655	105	0.41	1680	105	0.64
3	Definite			1526[a]	114[a]	0.57[a]	1548[a]	116[a]	0.326[a]	Possible			Definite			1692[a]	132[a]	0.68[a]
4	1466	211	0.658	1541	149	0.509	1591	(268)	0.696	-	-	-	1678	173	0.391	1687	177	0.56
5	1470	211	0.66	1520	114	0.57	1550	116	0.33	1730			1680	173	0.391	1690	132	0.68
6	1466	211	0.66	1526	115	0.57	1540	160	0.3	1680			1678	175	0.391	1692	130	0.68
7	1462	391	0.49	1512	106	0.45	1502	(36)	0.36	Not Present			1669	115	0.50	1685	104	0.54
8	1436	224	0.46	1512	125	0.49	1499	53	0.35	Not Present			1667	115	0.43	1684	123	0.54
Average	1468	244	0.61	1520	120	0.53	1535	118	0.39	1705			1672	142	0.42	1688	127	0.62
±	±19	±62	±.09	±10	±13	±.04	±28	±35	±.14	±25			±10	±29	±.04	±4	±22	±.06

Phase Shift* Analysis	S_{11} (1700)			P_{11} (1780)			P_{13} (1860)			F_{17} (1990)			D_{13} (2040)			G_{17}(2190)		
	M	Γ	x	M	Γ	x	M	Γ	x	M	Γ	x	M	Γ	x	M	Γ	x
1	1710	260	-	Probable			Ambiguous[b]			b			b			b		
2	1665	110	-	Probable			Ambiguous[b]			b			b			b		
3	1709[a]	300[a]	0.786[a]	Probable			Ambiguous[b]			b			b			b		
4	-	-	-	1751	327	0.32	1863	296	0.207	1983	225	0.128	2057	293	0.26	2265	298	0.349
5	1710	300	0.79	1750	327	0.32	1860	296	0.21	-	-	-	2030	290	0.11	2190	300	0.35
6	1709	300	0.79	1860	270	0.32	1900	325	0.25	1995	250	0.09	2040	240	0.15	2265	300	0.35
7	1766	404	0.56	1770	445	0.43	1844	449	0.40	c			b			(1906)[c]	(319)[c]	(0.14)[c]
8	1671	121	0.51	(1867)	(525)	0.30	1854	307	0.26	c			b			c		
9							1860	-	-	2000	-	-	2030	-	-	2000		
Average	1706	256	0.69	1783	350	0.34	1864	335	0.27	1989	238	0.109	2039	274	0.17	2180	299	0.350
±	±31	±98	±.13	±45	±63	±.05	±17	±58	±.07	±6	±12	±.019	±11	±24	±.06	±35	±2	±.001

TABLE I (cont'd.)

S = 0 Baryon Resonances

I = 3/2 States

Phase Shift* Analysis	S_{31} (1650)			P_{33} (1690)			D_{33} (1670)			F_{35} (1890)			P_{31} (1910)			D_{35} (1960)		
	M	Γ	x	M	Γ	x	M	Γ	x	M	Γ	x	M	Γ	x	M	Γ	x
1	1695	250	-	Ambiguous			Possible			Possible			Ambiguous[b]			Ambiguous[b]		
2	1650	130	-	Ambiguous			Possible			Possible			Ambiguous[b]			Ambiguous[b]		
3	Definite			Possible			Ambiguous			Probable			Probable[b]			b		
4	1635	177	0.284	1688	281	0.098	1691	269	0.14	1913	350	0.16	1934	339	0.30	1954	311	0.154
5	1640	177	0.28	1690	281	0.1	1690	269	0.14	1910	350	0.16	1930	339	0.3	-	-	-
6	1635	180	0.28	1690	240	0.08	1690	300	0.13	1910	380	0.15	1930	425	0.25	1970	400	0.12
7	1670	141	0.28	Not Present			1649	188	0.12	1841	136	0.2	1914	290	0.18	b		
8	1623	140	0.25	Not Present			1650	174	0.13	1852	150	0.19	1834	231	0.24	b		
9																1950	-	-
Average	1650	151	0.27	1689	267	0.93	1674	240	0.13	1885	273	0.17	1908	325	0.25	1958	356	0.14
±	±23	±89	±.12	±2	±19	±.09	±20	±50	±.01	±32	±107	±.02	±38	±64	±.04	±9	±44	±.02

	F_{37} (1950)			P_{33} (2160)		
	M	Γ	x	M	Γ	x
1	1975	180	0.57	b		
2	1980	140	-	b		
3	Definite			Possible[b]		
4	1946	221	0.386			
5	1950	221	0.39			
6	1946	220	0.39	2160	260	0.25
7	1935	221	0.51	b		
8	1935	212	0.39	b		
Average	1952	202	0.44	2160	260	0.25
±	±19	±29	±.07	-	-	-

* See Ref. 12. for various phase shift analyses

( ) Values in parentheses have not been used in the averages

(a) Values quoted by Lovelace, rapporteur talk at Heidelberg Conference (1967), p. 109.

(b) This state is very close to or beyond their highest energy

(c) Glasgow A has a G_{17} state at this mass, Glasgow B may have an F_{17} and a G_{17}; however, this energy is very close to their highest energy.

TABLE II

Magnet Currents and Central Field Values

Chamber	I(amps)	Field (KG)	Momentum Range(MeV/c)
72-inch	2,400	10.254	956-995
	2,600	11.025	1004-1024
	3,102	13.85	924
	3,690	14.54	1024-1042
	4,600	17.77	1125-1174
30-inch	12,000	20.98	556-853
	20,000	32.566	853-1602

Events Processed at Each Energy

Exposure	$E_{c.m}$ (MeV)	$p^{\pi^-}_{lab}$ (MeV/c)	4-C Events $\chi^2 \leq 14$	1-C $n\pi\pi$ events $\chi^2 \leq 8$	1-C $p\pi\pi$ events $\chi^2 \leq 8$
30"HBC(I)	1406	556	648	255	80
	1440	609	500	215	82
	1472	660	1110	418	245
	1496	699	1854	675	499
	1527	750	2337	832	701
	1556	797	826	340	272
	1589	853	997	579	387
	1709	1067	1141	585	400
	1730	1105	1954	1046	836
	1762	1165	2230	1231	899
30"HBC(II)	1811	1259	1544	1096	651
	1843	1322	2777	2172	1337
	1872	1381	2920	2443	1568
	1904	1444	3160	2616	1694
	1935	1509	1606	1288	886
30"HBC(III)	1720	1084	687	392	262
	1761	1161	1200	786	488
	1787	1212	1210	798	476
	1806	1250	292	188	122
	1821	1278	1740	1098	687
	1853	1340	2213	1649	979
	1885	1404	2392	1970	1180
	1916	1469	3792	3203	2105
	1933	1503	1972	1735	1177
	1963	1567	4113	3512	2405
	1980	1602	3957	3416	2458
				$\chi^2 \leq 7$	$\chi^2 \leq 7$
72"HBC	1628	924	537	358	200
	1647	956	5482	3169	1968
	1660	979	2697	1430	879
	1669	995	5127	2562	1603
	1674	1004	4966	2673	1568
	1685	1024	4398	2281	1409
	1695	1042	2206	1299	871
	1740	1125	3594	2259	1786
	1766	1174	1733	1120	854
TOTALS			79,911	51,477	33,880

TABLE IV

Azimuthal Correction Factors and Errors

$\cos\theta\ (\pi^-_{out}, \pi^-_{inc})$

$E_{c.m}$ (MeV)	0.9 to 0.95	0.8 to 0.9	0.7 to 0.8	-0.8 to 0.7	-1.0 to -0.8
1406	1.50 ±0.20	1.25 ±0.10	1.10 ±0.08	1.08 ±0.04	1.02 ±0.08
1440	1.50 ±0.20	1.25 ±0.10	1.10 ±0.08	1.08 ±0.04	1.02 ±0.08
1472	1.50 ±0.20	1.25 ±0.10	1.10 ±0.08	1.08 ±0.04	1.02 ±0.08
1496	1.45 ±0.18	1.20 ±0.08	1.02 ±0.07	1.05 ±0.04	1.02 ±0.10
1527	1.45 ±0.14	1.13 ±0.07	1.10 ±0.07	1.01 ±0.03	1.10 ±0.10
1556	1.60 ±0.22	1.25 ±0.10	1.12 ±0.10	1.06 ±0.04	1.10 ±0.13
1589	1.60 ±0.22	1.25 ±0.10	1.12 ±0.10	1.06 ±0.04	1.10 ±0.13
1628	1.30 ±0.20	1.08 ±0.12	1.12 ±0.20	1.0 ±0.07	1.18 ±0.18
1647	1.28 ±0.06	1.08 ±0.04	1.05 ±0.05	1.05 ±0.03	1.14 ±0.06
1660	1.14 ±0.07	1.02 ±0.05	1.01 ±0.07	1.05 ±0.04	1.17 ±0.08
1669	1.22 ±0.05	1.07 ±0.04	1.04 ±0.05	1.04 ±0.03	1.16 ±0.07
1674	1.17 ±0.05	1.08 ±0.04	1.00 ±0.05	1.11 ±0.03	1.15 ±0.07
1685	1.29 ±0.07	1.07 ±0.05	1.07 ±0.06	1.05 ±0.04	1.12 ±0.06
1695	1.25 ±0.08	1.13 ±0.06	1.07 ±0.08	1.02 ±0.04	1.04 ±0.08
1709	1.30 ±0.10	1.08 ±0.05	1.05 ±0.06	1.03 ±0.04	1.10 ±0.09
1720	1.22 ±0.10	1.04 ±0.07	1.02 ±0.08	1.10 ±0.07	1.00 ±0.11
1730	1.30 ±0.10	1.08 ±0.05	1.05 ±0.06	1.03 ±0.04	1.10 ±0.09
1740	1.24 ±0.06	1.10 ±0.04	1.05 ±0.05	1.07 ±0.03	1.20 ±0.09

TABLE IV (CONT'D)

Azimuthal Correction Factors and Errors

$\cos\theta\ (\pi^-_{out}, \pi^-_{inc})$

$E_{c.m}$ (MeV)	0.9 to 0.95	0.8 to 0.9	0.7 to 0.8	-0.8 to 0.7	-1.0 to -0.8
1761	1.22 ±0.10	1.04 ±0.07	1.02 ±0.08	1.10 ±0.07	1.00 ±0.11
1762	1.19 ±0.07	1.13 ±0.07	1.03 ±0.06	1.07 ±0.04	1.17 ±0.10
1766	1.18 ±0.08	1.06 ±0.06	1.04 ±0.07	1.01 ±0.05	1.20 ±0.15
1787	1.11 ±0.07	1.08 ±0.05	1.05 ±0.06	1.05 ±0.04	1.01 ±0.10
1806	1.11 ±0.07	1.08 ±0.05	1.05 ±0.06	1.05 ±0.04	1.01 ±0.10
1811	1.18 ±0.11	1.05 ±0.07	1.09 ±0.09	1.00 ±0.05	1.00 ±0.11
1821	1.11 ±0.07	1.08 ±0.05	1.05 ±0.06	1.05 ±0.04	1.01 ±0.10
1843	1.17 ±0.06	1.07 ±0.05	1.10 ±0.08	1.06 ±0.05	1.07 ±0.11
1853	1.10 ±0.07	1.02 ±0.05	1.07 ±0.08	1.06 ±0.05	1.04 ±0.13
1872	1.10 ±0.06	1.05 ±0.04	1.10 ±0.07	1.03 ±0.04	1.05 ±0.10
1885	1.12 ±0.07	1.05 ±0.06	1.04 ±0.08	1.06 ±0.06	1.10 ±0.14
1904	1.05 ±0.05	1.06 ±0.04	1.09 ±0.07	1.04 ±0.04	1.11 ±0.14
1916	1.25 ±0.06	1.08 ±0.05	1.15 ±0.08	1.11 ±0.05	1.00 ±0.11
1933	1.16 ±0.08	1.13 ±0.06	1.16 ±0.10	1.10 ±0.06	1.12 ±0.20
1935	1.08 ±0.08	1.00 ±0.06	1.08 ±0.09	1.10 ±0.07	1.15 ±0.25
1963	1.12 ±0.05	1.07 ±0.05	1.01 ±0.01	1.05 ±0.04	1.15 ±0.15
1980	1.22 ±0.06	1.20 ±0.07	1.10 ±0.08	1.09 ±0.04	1.05 ±0.15

TABLE V

Legendre Coefficients

$$\frac{d\sigma}{d\Omega} = \sum_n A_n P_n(\cos\theta)$$

E_{cm} (MeV)	1406	1440	1472	1496	1527	1556	1589	1628	1647	1660
Low Energy Cut Off	1394	1428	1456	1482	1514	1544	1576	1616	1632	1648
High Energy Cut Off	1418	1452	1486	1510	1540	1568	1602	1640	1662	1672
A_0	0.82 ±0.05	1.02 ±0.08	1.22 ±0.06	1.52 ±0.06	1.58 ±0.06	1.19 ±0.08	1.15 ±0.07	1.50 ±0.11	1.72 ±0.04	1.84 ±0.04
A_1	0.61 ±0.12	1.09 ±0.19	1.48 ±0.16	2.23 ±0.15	2.45 ±0.15	1.45 ±0.19	1.22 ±0.17	1.43 ±0.26	1.85 ±0.09	1.85 ±0.13
A_2	0.54 ±0.17	1.31 ±0.27	1.66 ±0.22	2.42 ±0.21	2.61 ±0.20	1.52 ±0.27	1.69 ±0.24	3.04 ±0.36	3.65 ±0.12	4.06 ±0.17
A_3	-0.46 ±0.21	-0.04 ±0.31	-0.08 ±0.25	0.41 ±0.24	0.69 ±0.22	0.36 ±0.30	1.04 ±0.25	2.21 ±0.38	3.17 ±0.12	3.57 ±0.17
A_4	-0.16 ±0.19	0.00 ±0.27	0.03 ±0.21	0.07 ±0.19	-0.10 ±0.18	-0.30 ±0.25	-0.14 ±0.21	0.78 ±0.30	1.16 ±0.10	1.26 ±0.14
A_5	0.00 ±0.17	0.20 ±0.23	0.08 ±0.17	0.20 ±0.15	0.07 ±0.14	0.39 ±0.21	0.39 ±0.18	1.11 ±0.30	1.72 ±0.10	1.82 ±0.14
A_6										
χ^2	13.37	16.18	6.85	9.21	14.00	10.31	12.7	9.75	11.89	4.86
$\langle\chi^2\rangle$	13	13	13	13	13	13	13	13	14	14
Confidence Level (%)	42.0	23.9	91.0	75.7	37.4	66.9	47.2	71.4	61.5	98.8

TABLE V (Cont'd)

Legendre Coefficients

$$\frac{d\sigma}{d\Omega} = \sum_n A_n P_n(\cos\theta)$$

E_{cm}	1669	1674	1685	1695	1709	1720	1730	1740	1761	1762
Low Energy Cut Off	1656	1658	1670	1680	1696	1708	1716	1722	1750	1748
High Energy Cut Off	1682	1690	1700	1710	1720	1732	1744	1758	1772	1776
A_0	2.10 ±0.05	1.93 ±0.04	2.09 ±0.06	2.07 ±0.07	1.88 ±0.09	1.55 ±0.11	1.43 ±0.06	1.46 ±0.04	1.09 ±0.06	1.19 ±0.04
A_1	2.42 ±0.11	2.13 ±0.11	2.44 ±0.16	2.69 ±0.18	2.67 ±0.24	2.35 ±0.28	2.07 ±0.16	2.30 ±0.10	1.68 ±0.17	1.89 ±0.11
A_2	4.94 ±0.15	4.38 ±0.15	5.07 ±0.21	5.22 ±0.24	4.75 ±0.31	3.95 ±0.38	3.40 ±0.21	3.65 ±0.13	2.61 ±0.22	2.86 ±0.15
A_3	4.50 ±0.15	4.04 ±0.17	4.44 ±0.23	4.77 ±0.27	4.10 ±0.34	3.45 ±0.44	2.98 ±0.23	3.01 ±0.15	2.26 ±0.25	2.38 ±0.16
A_4	1.83 ±0.12	1.64 ±0.17	2.00 ±0.22	2.18 ±0.25	2.01 ±0.31	1.69 ±0.42	1.37 ±0.21	1.62 ±0.14	1.08 ±0.24	1.29 ±0.16
A_5	2.13 ±0.12	1.98 ±0.13	2.08 ±0.15	2.16 ±0.17	1.53 ±0.22	1.20 ±0.30	1.07 ±0.16	1.06 ±0.10	0.89 ±0.18	0.72 ±0.12
A_6		0.14 ±0.13	-0.04 ±0.15	0.17 ±0.17	-0.28 ±0.21	0.32 ±0.29	-0.37 ±0.14	-0.14 ±0.10	-0.14 ±0.16	-0.17 ±0.11
χ^2	20.09	14.75	14.91	9.23	9.86	14.78	6.52	10.45	8.83	15.1
$\langle\chi^2\rangle$	14	13	13	13	13	13	13	13	13	13
Confidence Level	12.7	32.3	31.3	75.5	70.5	32.2	92.5	65.7	78.5	30.2

TABLE V (Cont'd)

Legendre Coefficients

$$\frac{d\sigma}{d\Omega} = \sum_n A_n P_n(\cos\,\theta)$$

E_{cm}	1766	1787	1806	1811	1821	1843	1853	1872	1885	1904
Low Energy Cut Off	1754	1774	1794	1796	1808	1828	1838	1856	1872	1890
High Energy Cut Off	1778	1800	1818	1826	1834	1858	1866	1888	1898	1918
A_0	1.25 ±0.05	0.99 ±0.05	1.06 ±0.09	1.10 ±0.05	1.02 ±0.04	1.04 ±0.04	0.99 ±0.04	1.00 ±0.03	0.98 ±0.04	0.95 ±0.03
A_1	2.08 ±0.13	1.62 ±0.13	1.82 ±0.22	1.82 ±0.13	1.71 ±0.12	1.80 ±0.10	1.67 ±0.10	1.73 ±0.08	1.74 ±0.11	1.74 ±0.08
A_2	3.15 ±0.18	2.33 ±0.17	2.76 ±0.31	2.64 ±0.18	2.38 ±0.16	2.52 ±0.13	2.34 ±0.13	2.37 ±0.11	2.39 ±0.15	2.36 ±0.11
A_3	2.73 ±0.20	1.94 ±0.19	2.35 ±0.35	2.30 ±0.19	2.14 ±0.18	2.28 ±0.14	2.17 ±0.14	2.31 ±0.12	2.37 ±0.16	2.40 ±0.11
A_4	1.61 ±0.19	0.79 ±0.18	1.28 ±0.34	1.26 ±0.18	1.12 ±0.17	1.31 ±0.13	1.32 ±0.14	1.45 ±0.11	1.60 ±0.14	1.67 ±0.10
A_5	1.03 ±0.14	0.41 ±0.14	0.64 ±0.26	0.53 ±0.14	0.50 ±0.13	0.61 ±0.10	0.52 ±0.11	0.56 ±0.09	0.64 ±0.11	0.76 ±0.08
A_6	0.07 ±0.13	-0.29 ±0.12	-0.03 ±0.25	-0.11 ±0.12	-0.10 ±0.11	-0.06 ±0.09	-0.03 ±0.10	0.11 ±0.08	0.21 ±0.09	0.25 ±0.07
χ^2	13.73	12.85	12.20	9.71	7.38	15.87	9.40	9.69	8.34	10.67
$\langle\chi^2\rangle$	13	13	13	13	13	13	13	13	13	13
Confidence Level	39.3	45.9	51.1	71.8	88.1	25.6	74.2	71.9	82.1	63.9

TABLE V (Cont'd)

Legendre Coefficients

$$\frac{d\sigma}{d\Omega} = \sum_n A_n P_n(\cos\theta)$$

E_{cm}	1916	1933	1935	1963	1980					
Low Energy Cut Off	1902	1917	1920	1948	1966					
High Energy Cut Off	1930	1947	1950	1978	1994					
A_0	0.87 ±0.03	0.93 ±0.04	0.83 ±0.04	0.81 ±0.02	0.78 ±0.03					
A_1	1.59 ±0.08	1.79 ±0.10	1.53 ±0.10	1.56 ±0.06	1.56 ±0.07					
A_2	2.05 ±0.11	2.40 ±0.14	2.02 ±0.14	2.09 ±0.09	2.01 ±0.10					
A_3	2.13 ±0.11	2.55 ±0.15	2.13 ±0.15	2.20 ±0.09	2.15 ±0.10					
A_4	1.37 ±0.10	1.79 ±0.13	1.47 ±0.13	1.65 ±0.09	1.59 ±0.09					
A_5	0.52 ±0.08	0.87 ±0.10	0.68 ±0.11	0.84 ±0.07	0.80 ±0.07					
A_6	0.20 ±0.06	0.41 ±0.09	0.34 ±0.09	0.45 ±0.05	0.37 ±0.05					
χ^2	13.96	7.82	3.00	12.44	7.31					
$\langle\chi^2\rangle$	13	13	13	13	13					
Confidence Level	37.6	85.5	99.8	49.2	88.5					

FIGURE CAPTIONS

1. Scope of the present experiment. Solid lines mark energies where data has been analyzed. Dashed lines mark energies to which the experiment will be extended.

2. Argonne beam optics.

   (a) - (b) Vertical and horizontal planes of the optics used for the second and third exposures.

   (c) Simplified mode used for the first exposure.

3. Berkeley beam.

4. Beam track pull quantities for each exposure:

   (a) - (c) 30-inch HBC

   (d) 72-inch HBC.

5. Missing mass squared in the reaction $\pi^- p \rightarrow \pi^- pmm$ for the 4C elastic events. The shift toward the negative side is expected in such missing mass plots.[19]

6. Center-of-mass energies from 4C events for typical roll regions of the film. Shading indicates the data used in the analysis.

7. Number of events of the three reaction types processed at each energy.

8. χ^2 distributions for each exposure:

   (a) - (c) 30-inch HBC

   (d) 72-inch HBC.

   Smooth curves are the scaled theoretical distributions normalized to the total number of events.

9. Azimuthal angle for forward, middle, and backward regions of pion production angle. α is defined as the angle between the normal to the scattering plane and the camera axis.

10. π^-p elastic cross section measurements of Duke _et al._,[20] Helland _et al._,[21] Ogden et al.,[22] and this experiment. The lower curve is the cross section integrated over the region used for normalization, $-0.8 \leq \cos\theta \leq 0.7$. The arrows indicate energies chosen for comparison of differential cross sections with the results of phase shift analyses.

11. π^-p differential cross sections measured in this experiment. Smooth curves represent the best fit by an expansion in Legendre polynomials.

12. Legendre coefficients from fit to π^-p differential cross sections.

13. Forward π^-p elastic cross section measured in this experiment. The smooth curve is calculated by Carter[24] using dispersion relations and the total π^-p cross section measurements of Carter _et al._[25]

14. Total π^-p cross sections measured by Carter _et al._,[25] Berkeley,[26] Princeton,[27] Saclay (1961),[28] and Saclay (1966).[29]

15. π^-p elastic cross section measurements of Duke _et al._,[20] Helland _et al._,[21] Ogden _et al._,[22] and this experiment. Solid and dashed lines represent the π^-p elastic cross section predicted by CERN-EXPT and CERN-TH phase shifts, respectively. The arrows indicate the energies chosen for differential cross section comparison.

16. π^-p differential cross section at six energies measured in this experiment. Solid and dashed lines are the predictions of CERN-EXPT and CERN-TH phase shifts.

17. π^-p elastic cross section predicted by Saclay,[1] Berkeley,[6] and Glasgow,[31] compared to the same data as Fig. 18.

18. π^-p differential cross section predicted by Saclay,[1] Berkeley,[6] and Glasgow,[31] compared to the experimental data.

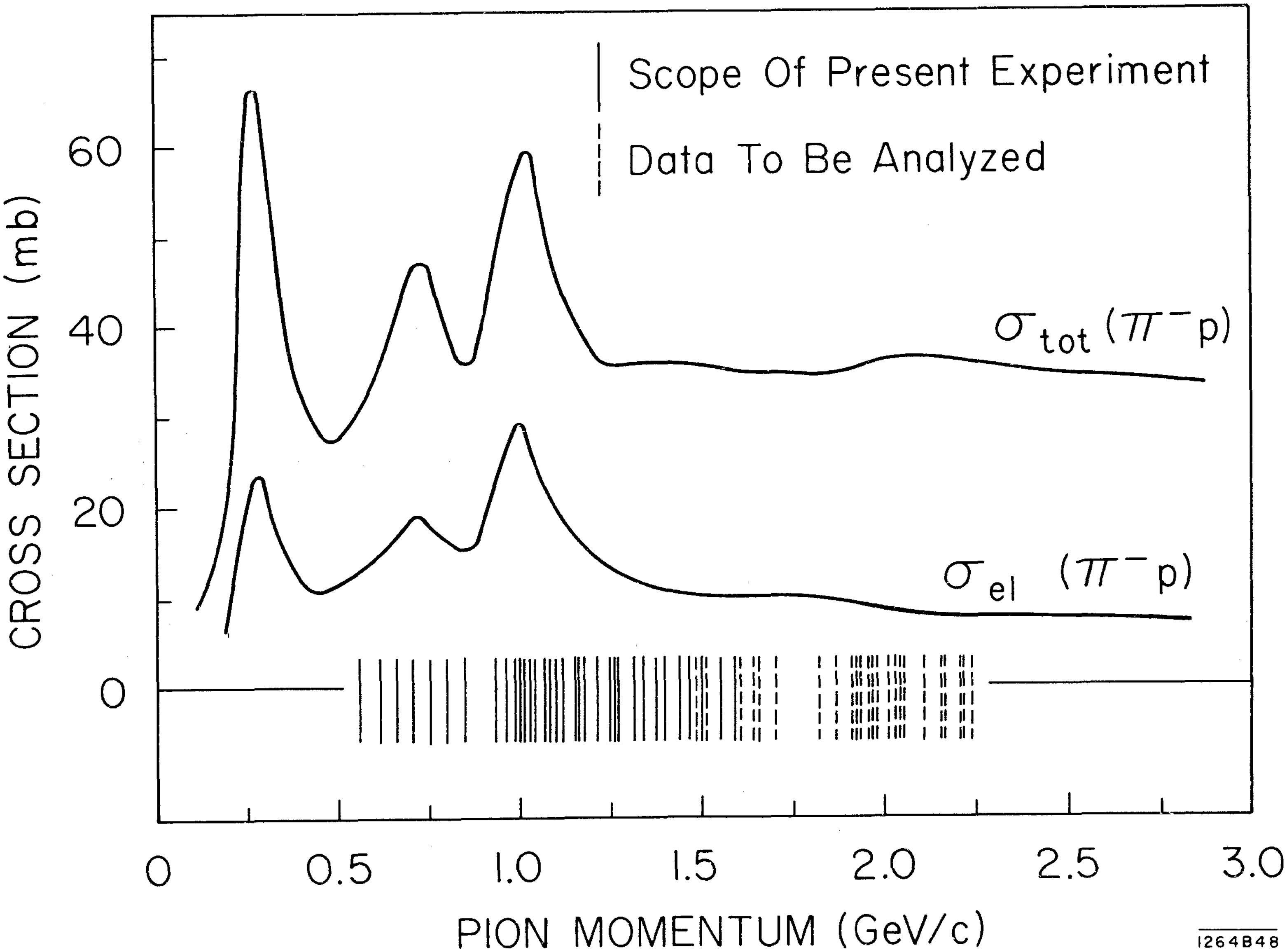

Scope Of Present Experiment
Data To Be Analyzed
$\sigma_{tot}(\pi^- p)$
$\sigma_{el}\ (\pi^- p)$
CROSS SECTION (mb)
0
20
40
60
0
0.5
1.0
1.5
2.0
2.5
3.0
PION MOMENTUM (GeV/c)
1264B48

Fig. 1

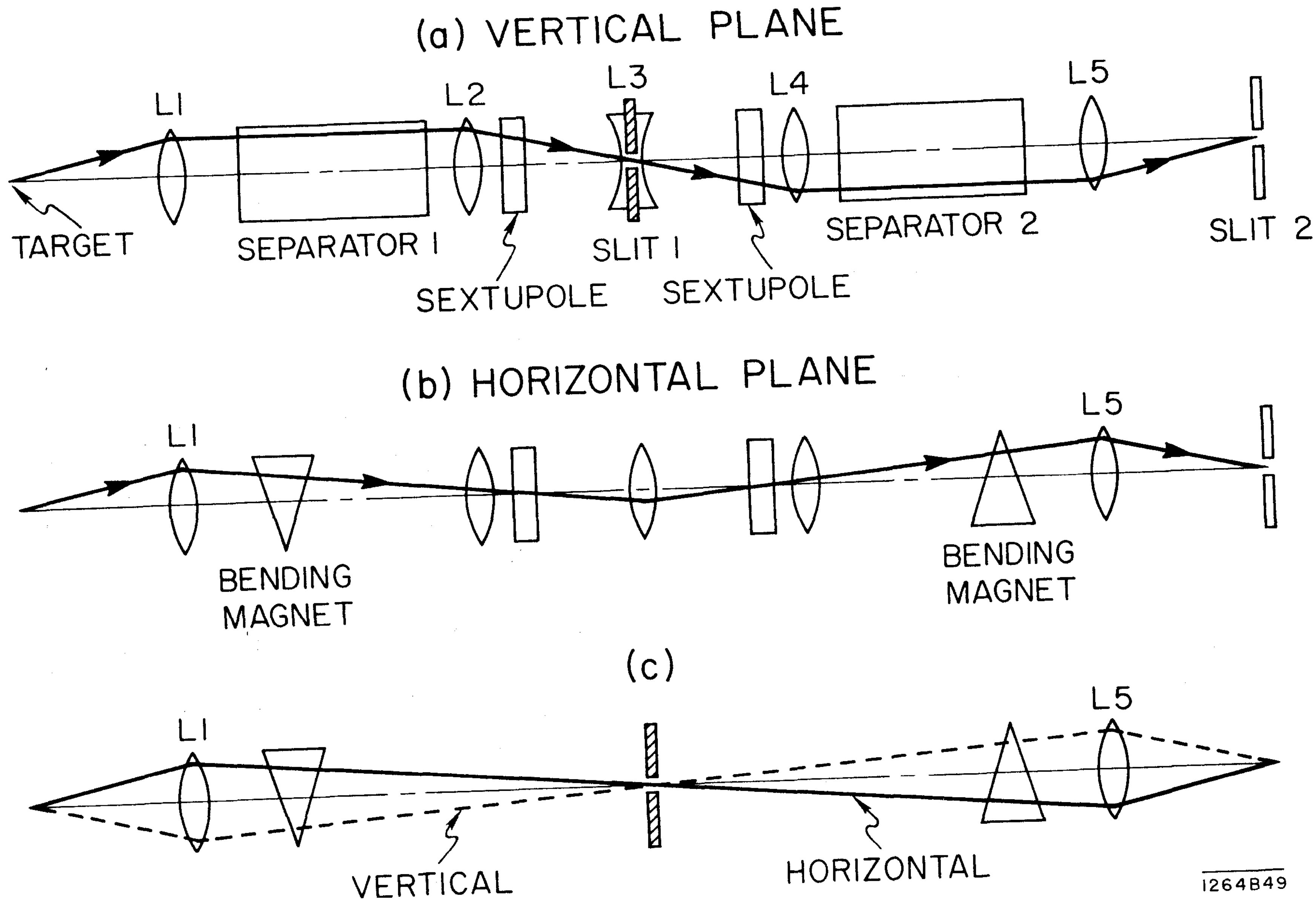
(a) VERTICAL PLANE
L1
L2
L3
L4
L5
TARGET
SEPARATOR 1
SEXTUPOLE
SLIT 1
SEXTUPOLE
SEPARATOR 2
SLIT 2
(b) HORIZONTAL PLANE
L1
L5
BENDING MAGNET
BENDING MAGNET
(c)
L1
L5
VERTICAL
HORIZONTAL
1264B49

Fig. 2

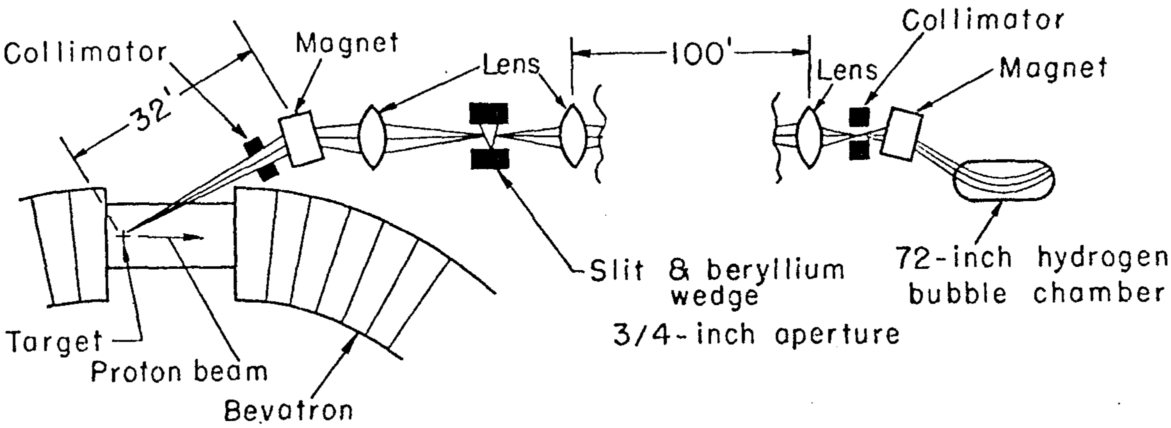

1264A51

Fig. 3

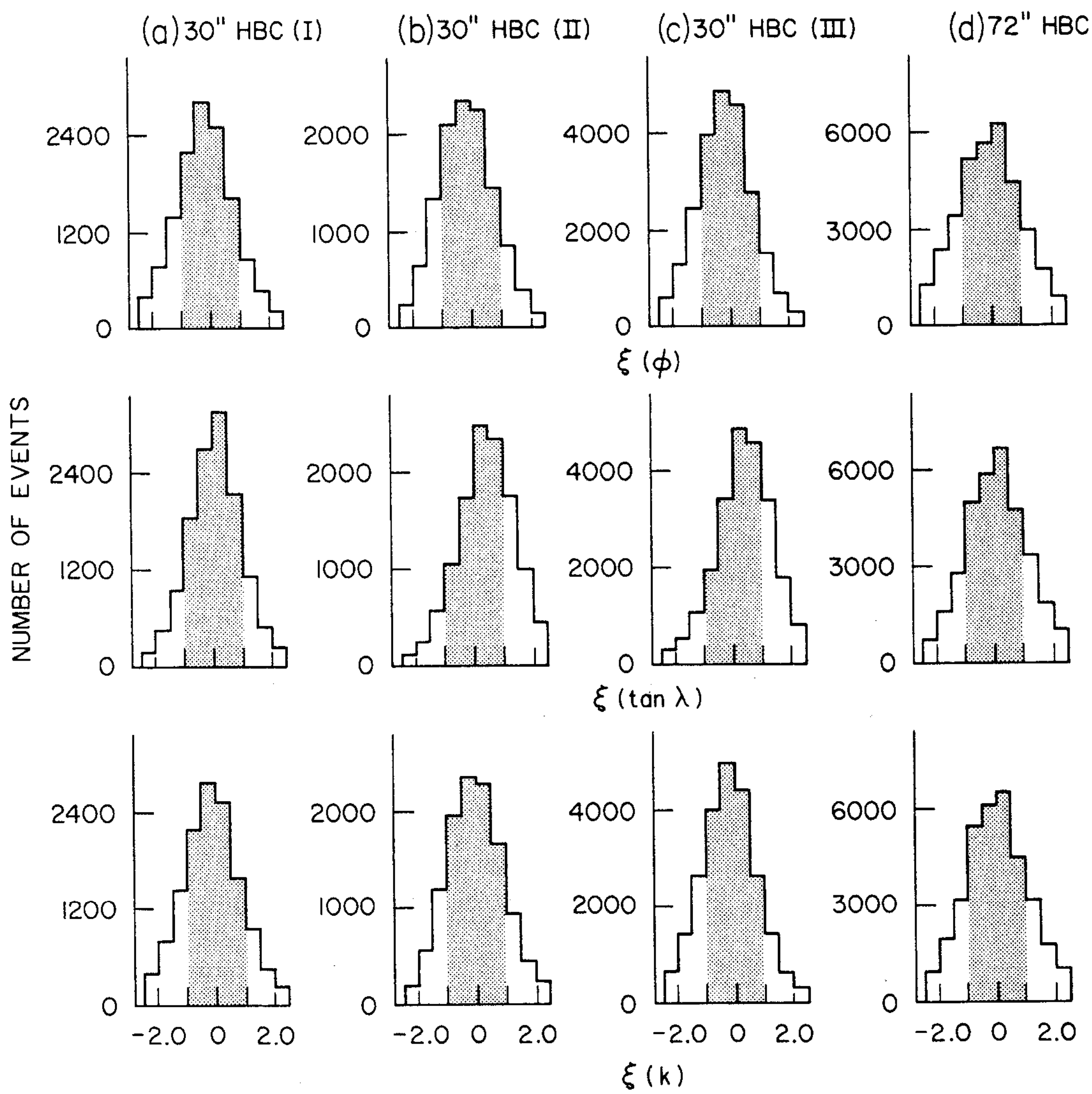

$$\xi(X) = \frac{(X_{meas} - X_{fit})}{\langle X_{meas} - X_{fit} \rangle}$$

1264C44

Fig. 4

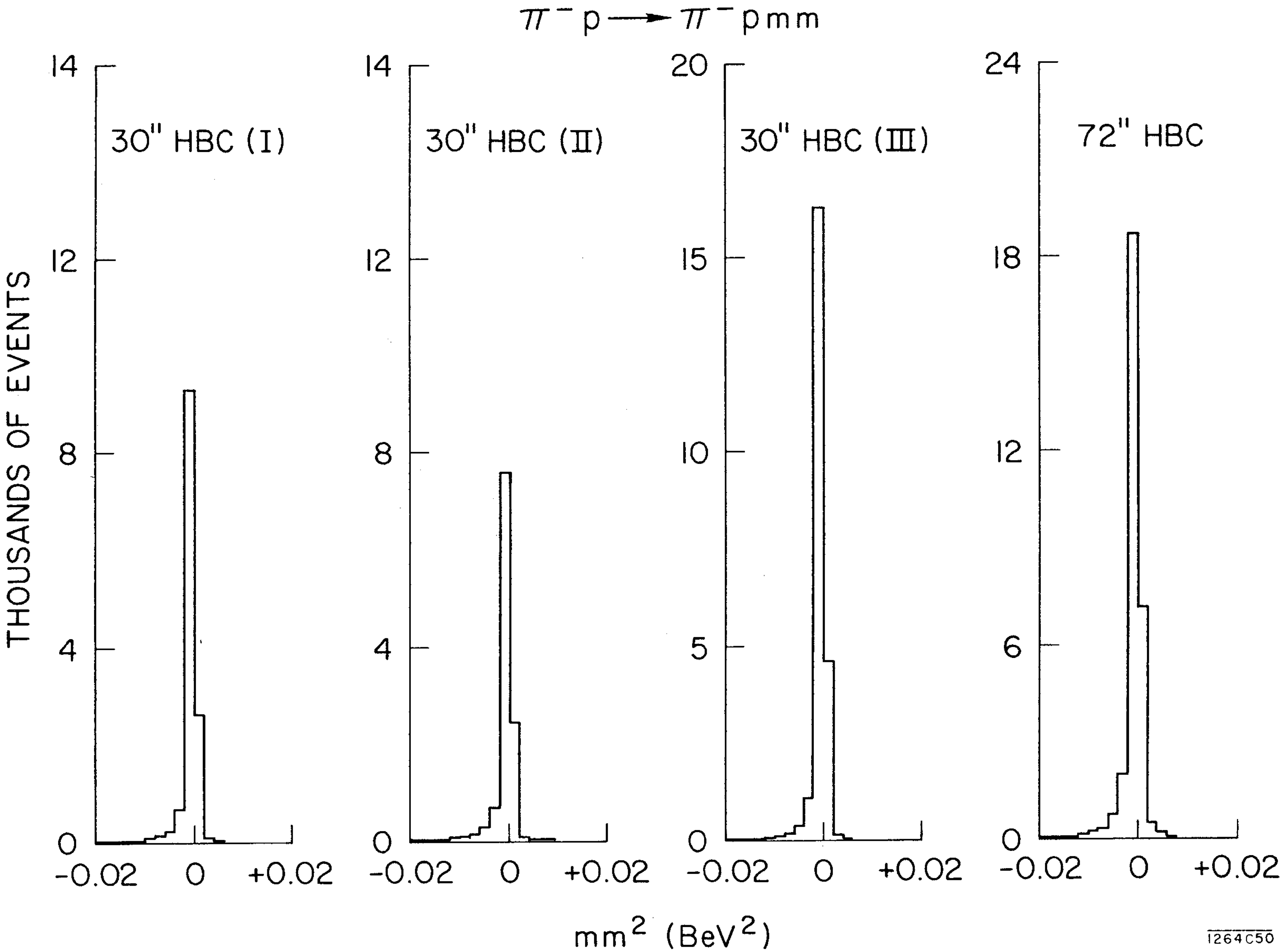

$\pi^- p \to \pi^- p mm$
THOUSANDS OF EVENTS
30" HBC (I)
30" HBC (II)
30" HBC (III)
72" HBC
14
12
8
4
0
14
12
8
4
0
20
15
10
5
0
24
18
12
6
0
-0.02
0
+0.02
-0.02
0
+0.02
-0.02
0
+0.02
-0.02
0
+0.02
mm^2 (BeV^2)
1264C50

Fig. 5

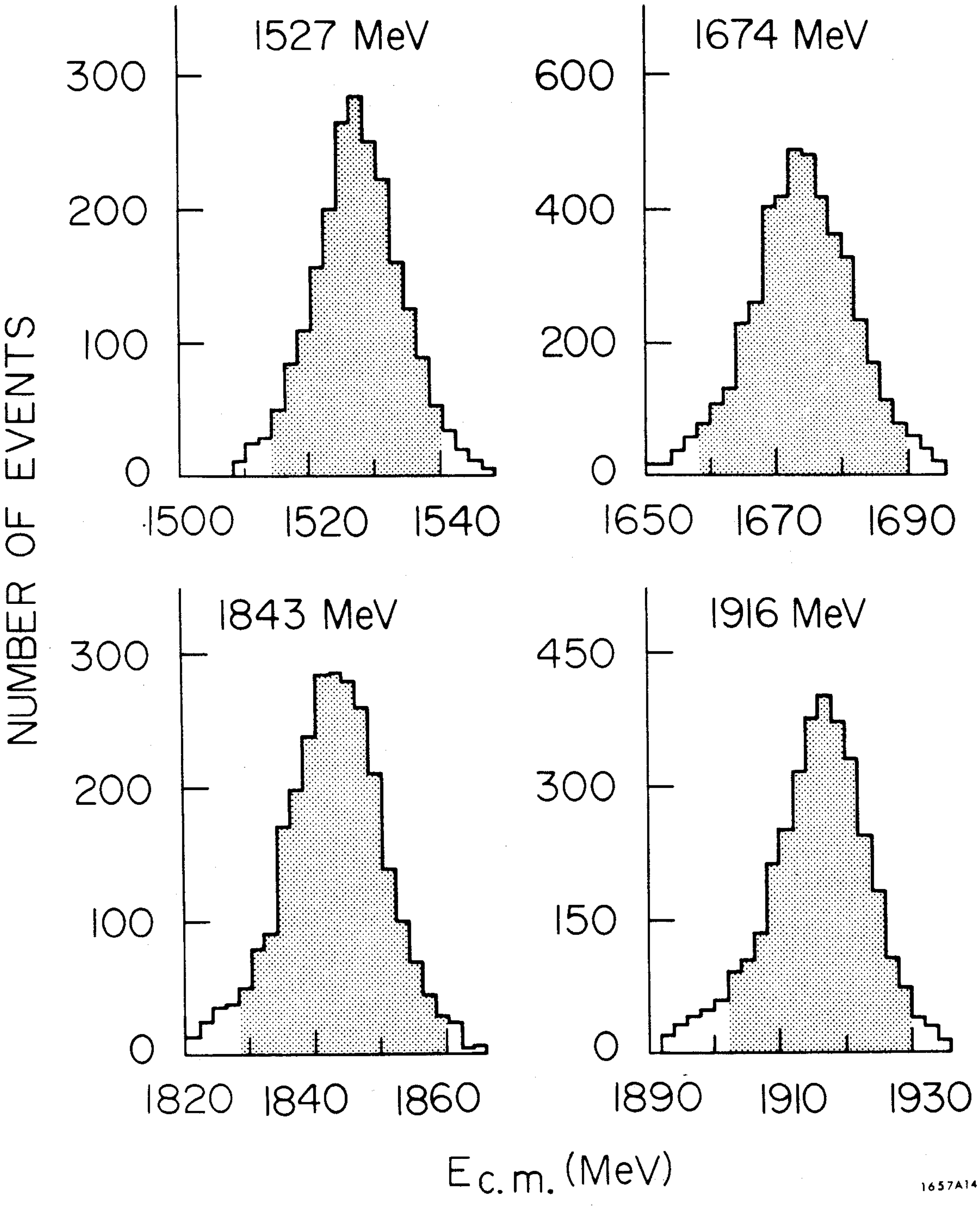
1527 MeV
1674 MeV
1843 MeV
1916 MeV
NUMBER OF EVENTS
300
200
100
0
600
400
200
0
300
200
100
0
450
300
150
0
1500
1520
1540
1650
1670
1690
1820
1840
1860
1890
1910
1930
Ec.m. (MeV)
1657A14

Fig. 6

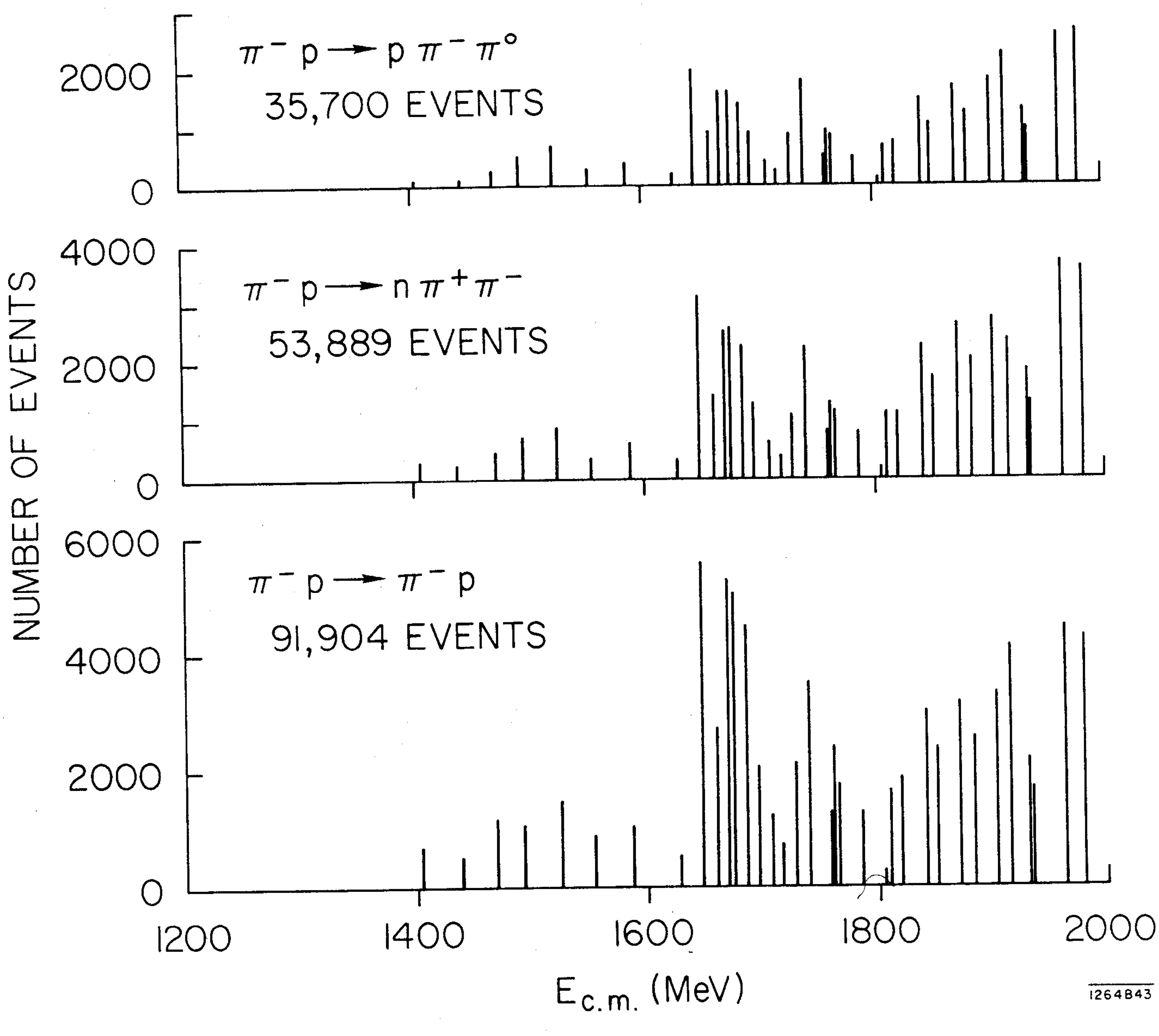

π⁻ p → p π⁻ π°
35,700 EVENTS
π⁻ p → n π⁺ π⁻
53,889 EVENTS
π⁻ p → π⁻ p
91,904 EVENTS
NUMBER OF EVENTS
0
2000
4000
6000
1200
1400
1600
1800
2000
E c.m. (MeV)
1264B43

Fig. 7

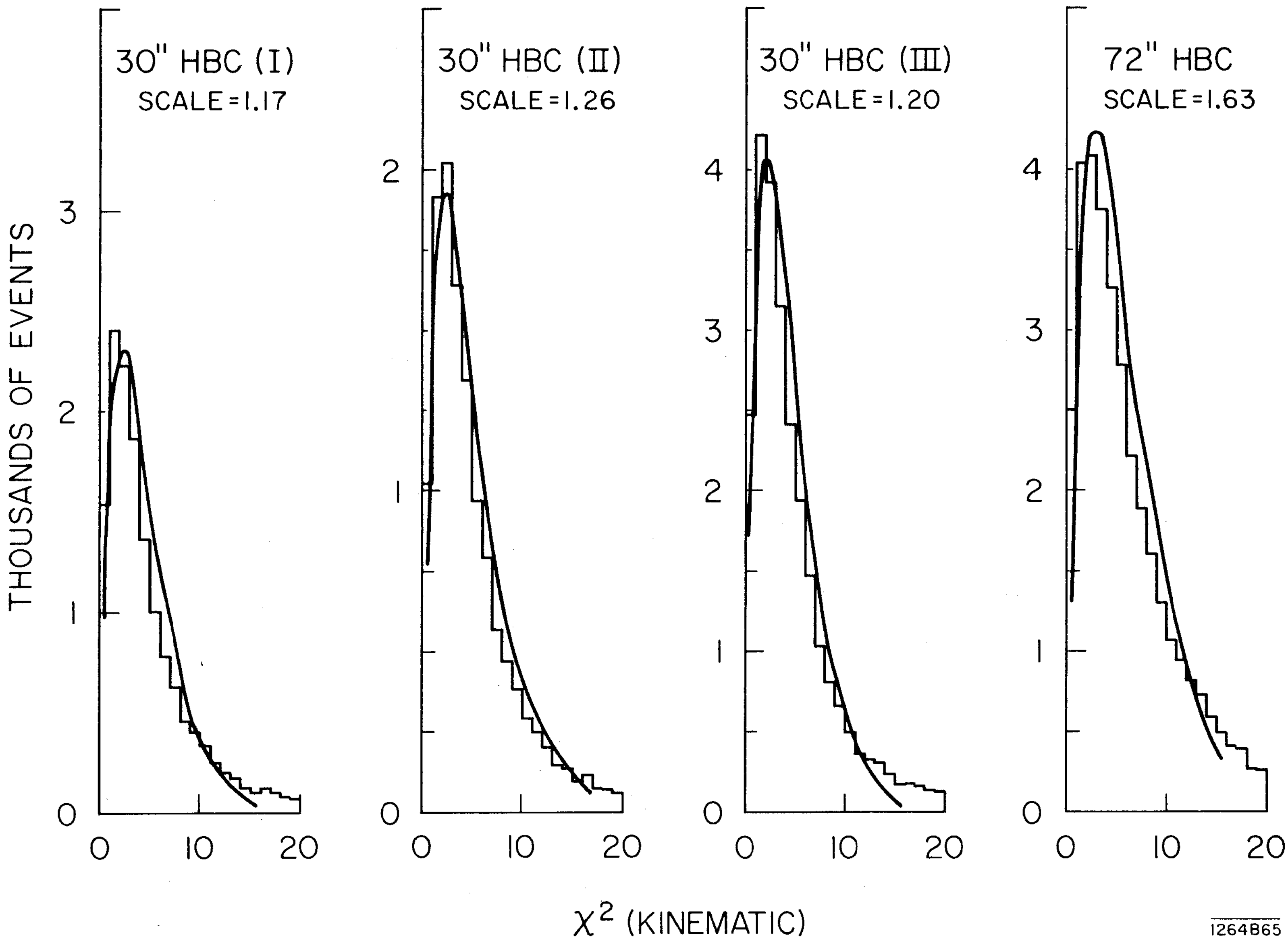

30" HBC (I)
SCALE=1.17
30" HBC (II)
SCALE=1.26
30" HBC (III)
SCALE=1.20
72" HBC
SCALE=1.63
THOUSANDS OF EVENTS
0
1
2
3
4
10
20
χ² (KINEMATIC)
1264B65

Fig. 8

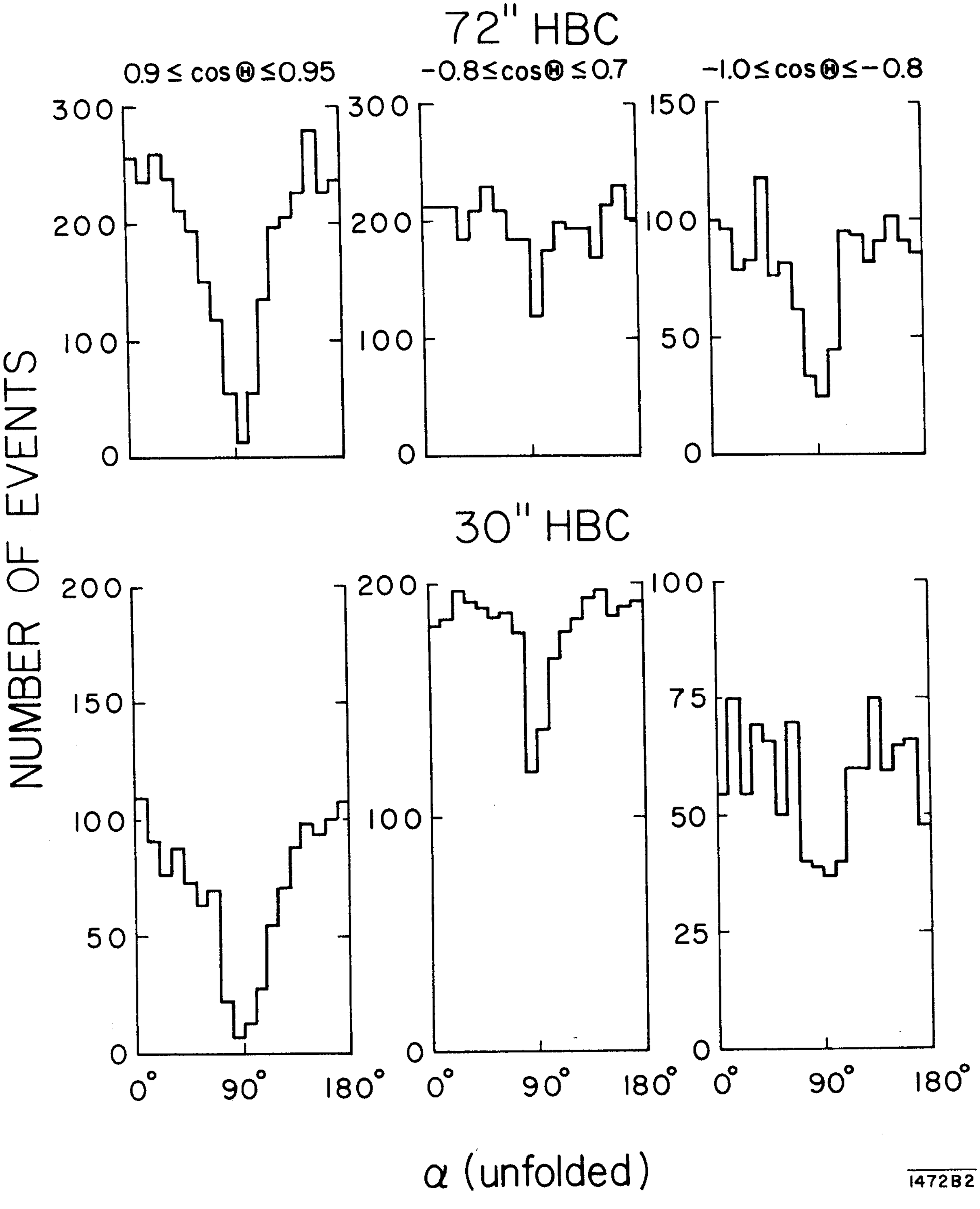

72" HBC
0.9 ≤ cos Θ ≤ 0.95
−0.8 ≤ cos Θ ≤ 0.7
−1.0 ≤ cos Θ ≤ −0.8
300
200
100
0
150
50
30" HBC
NUMBER OF EVENTS
200
150
100
50
0
75
25
0°
90°
180°
α (unfolded)
147282

Fig. 9

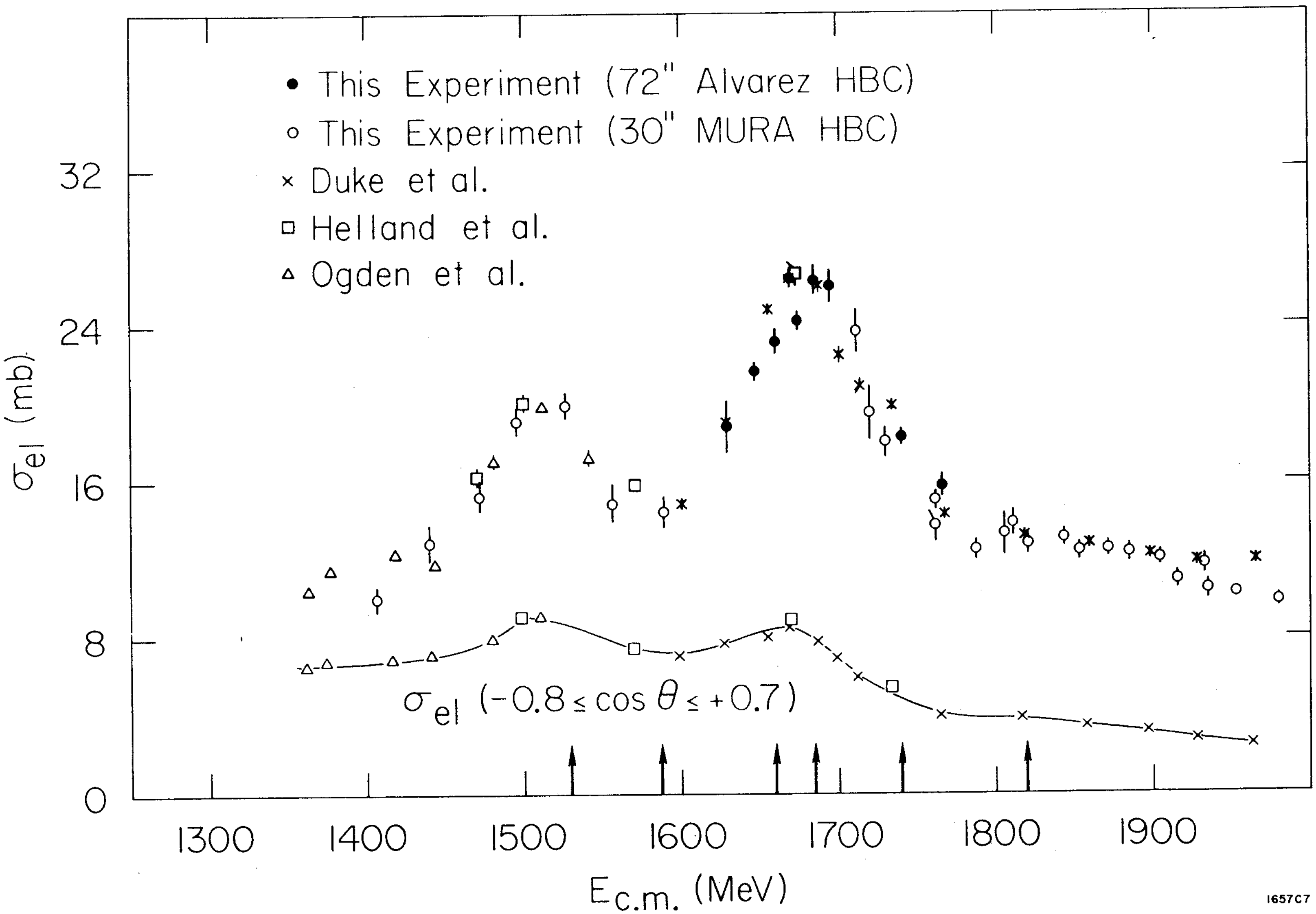

This Experiment (72" Alvarez HBC)
This Experiment (30" MURA HBC)
Duke et al.
Helland et al.
Ogden et al.
32
24
16
8
0
σ_{el} (mb)
σ_{el} $(-0.8 \leq \cos\theta \leq +0.7)$
1300
1400
1500
1600
1700
1800
1900
$E_{c.m.}$ (MeV)
1657C7

Fig. 10

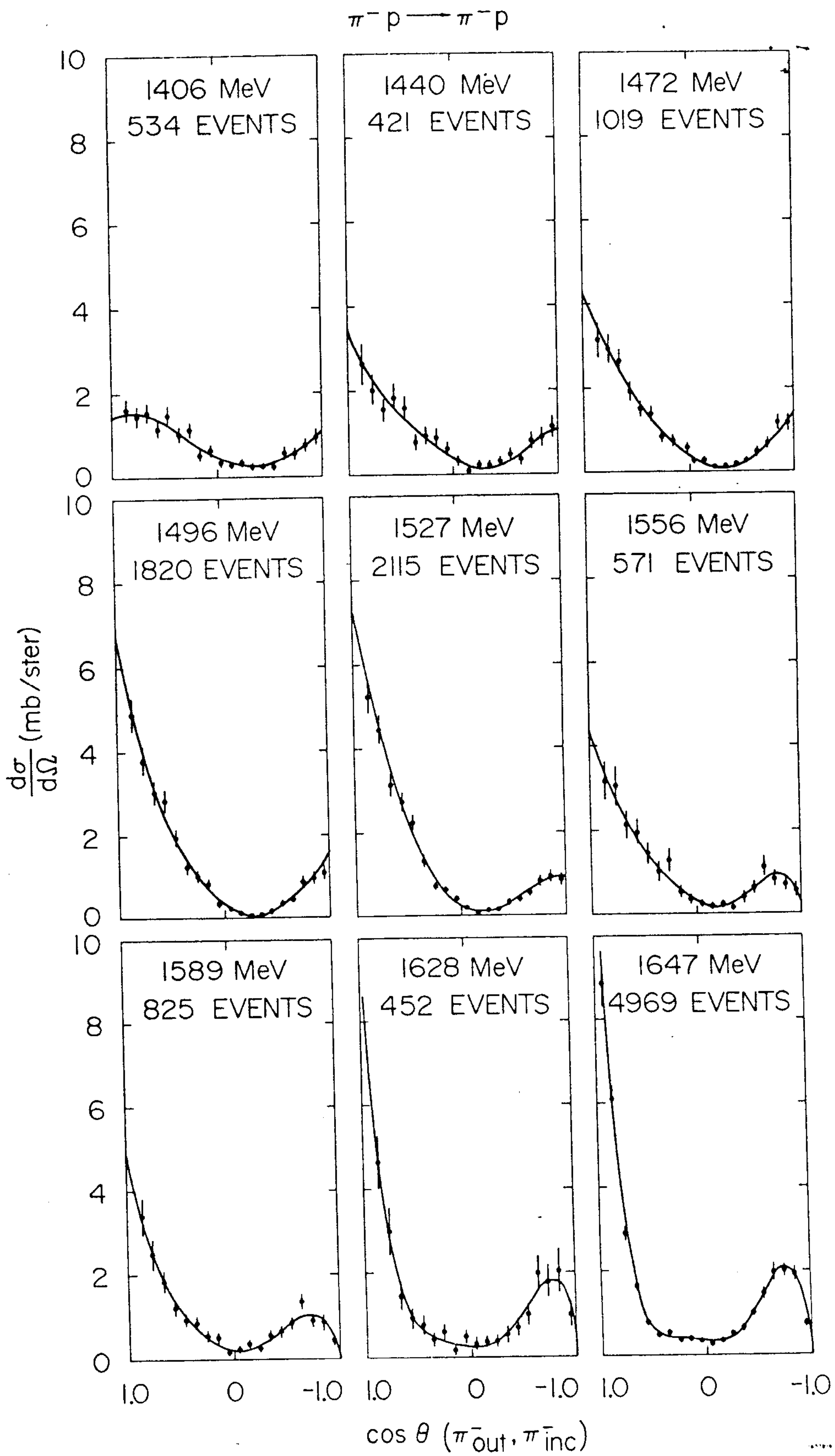

π⁻ p ⟶ π⁻ p
1406 MeV
534 EVENTS
1440 MeV
421 EVENTS
1472 MeV
1019 EVENTS
1496 MeV
1820 EVENTS
1527 MeV
2115 EVENTS
1556 MeV
571 EVENTS
1589 MeV
825 EVENTS
1628 MeV
452 EVENTS
1647 MeV
4969 EVENTS
dσ/dΩ (mb/ster)
cos θ (π⁻out, π⁻inc)

Fig. 11

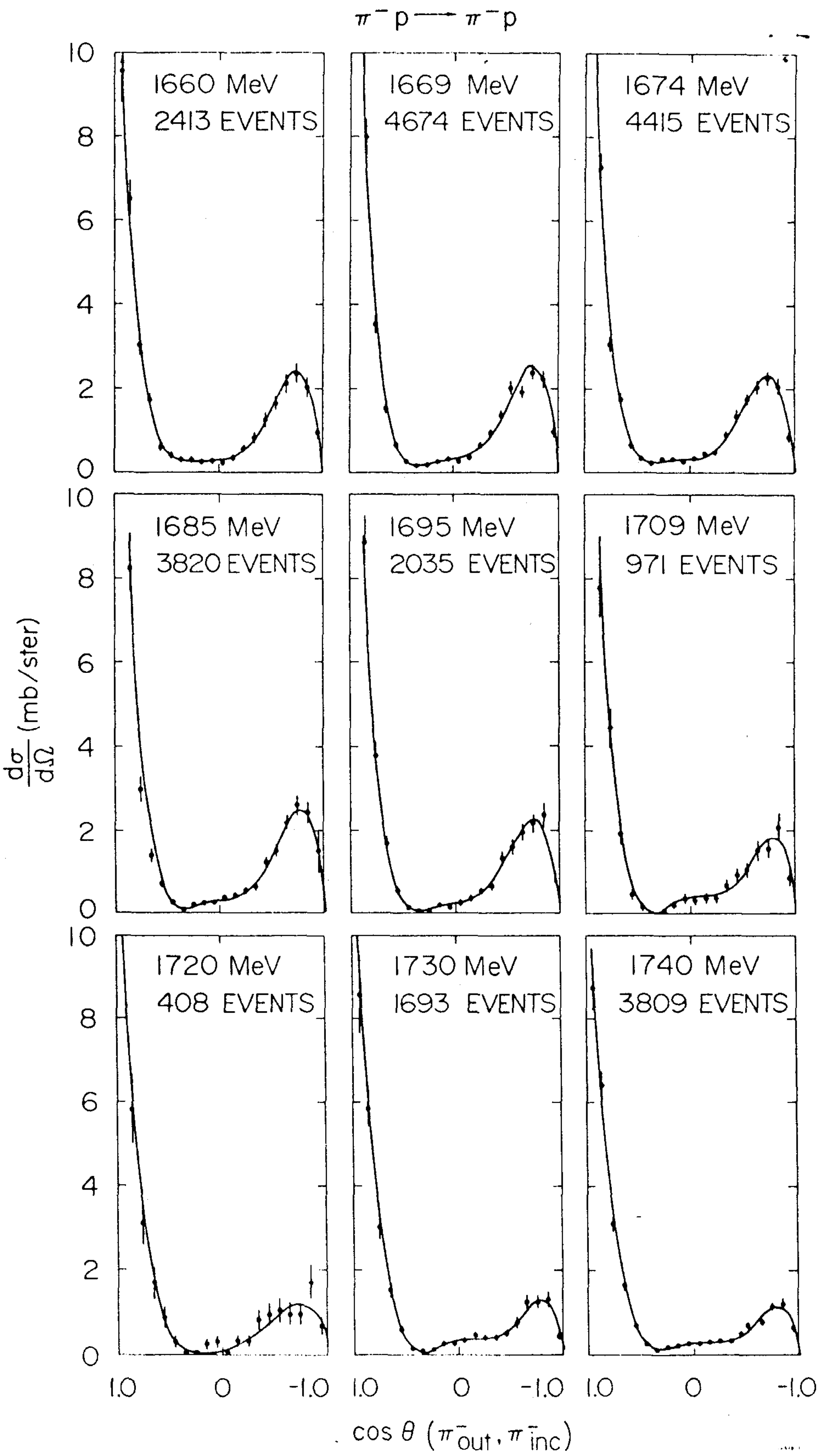

$\pi^- p \longrightarrow \pi^- p$
1660 MeV
2413 EVENTS
1669 MeV
4674 EVENTS
1674 MeV
4415 EVENTS
1685 MeV
3820 EVENTS
1695 MeV
2035 EVENTS
1709 MeV
971 EVENTS
1720 MeV
408 EVENTS
1730 MeV
1693 EVENTS
1740 MeV
3809 EVENTS
$\frac{d\sigma}{d\Omega}$ (mb/ster)
0
2
4
6
8
10
1.0
0
-1.0
$\cos\theta\ (\pi^-_{out}, \pi^-_{inc})$

Fig. 11

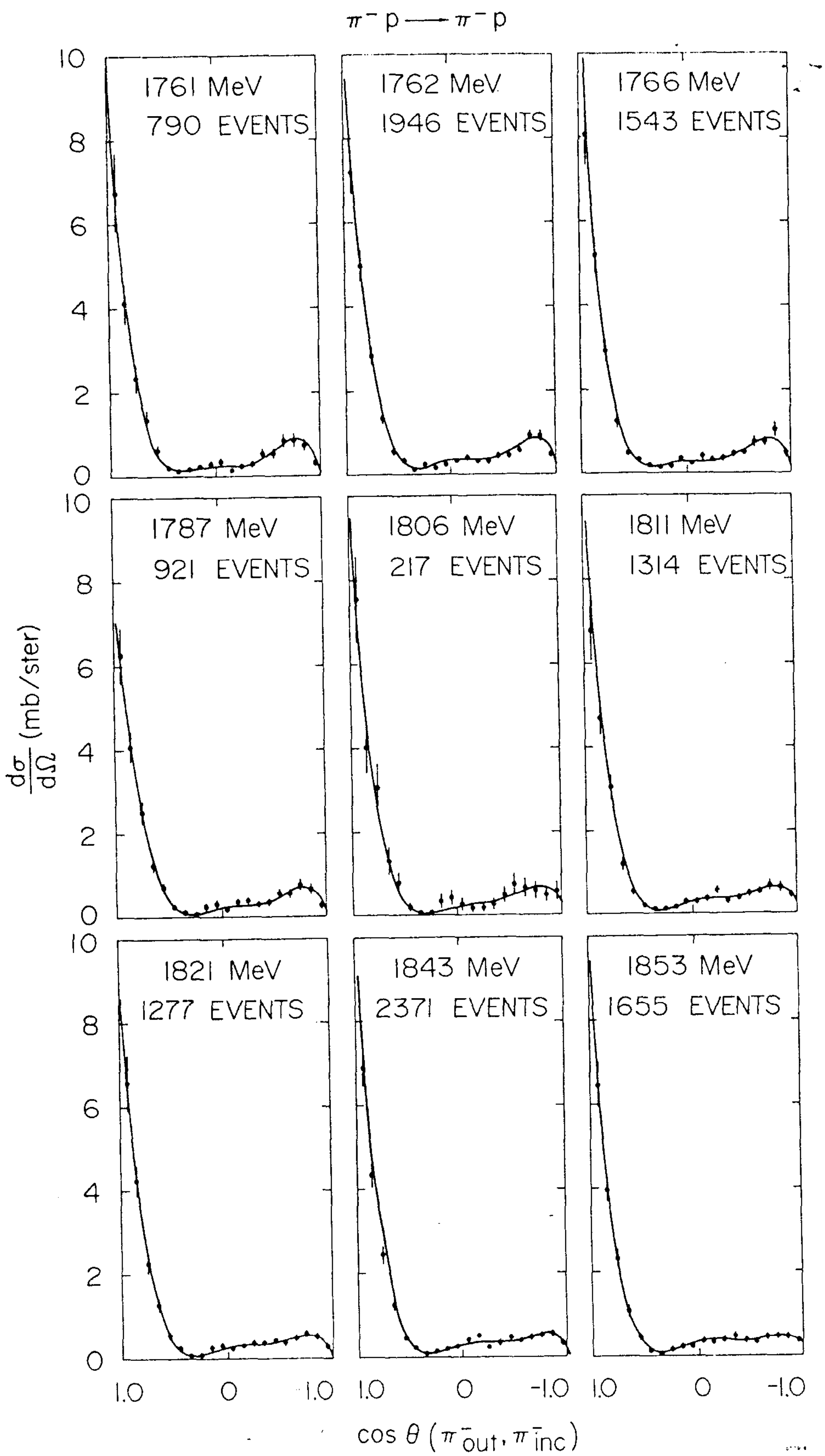

π⁻ p ⟶ π⁻ p
1761 MeV
790 EVENTS
1762 MeV
1946 EVENTS
1766 MeV
1543 EVENTS
1787 MeV
921 EVENTS
1806 MeV
217 EVENTS
1811 MeV
1314 EVENTS
1821 MeV
1277 EVENTS
1843 MeV
2371 EVENTS
1853 MeV
1655 EVENTS
dσ/dΩ (mb/ster)
10
8
6
4
2
0
1.0
0
-1.0
cos θ (π⁻out, π⁻inc)

Fig. 11

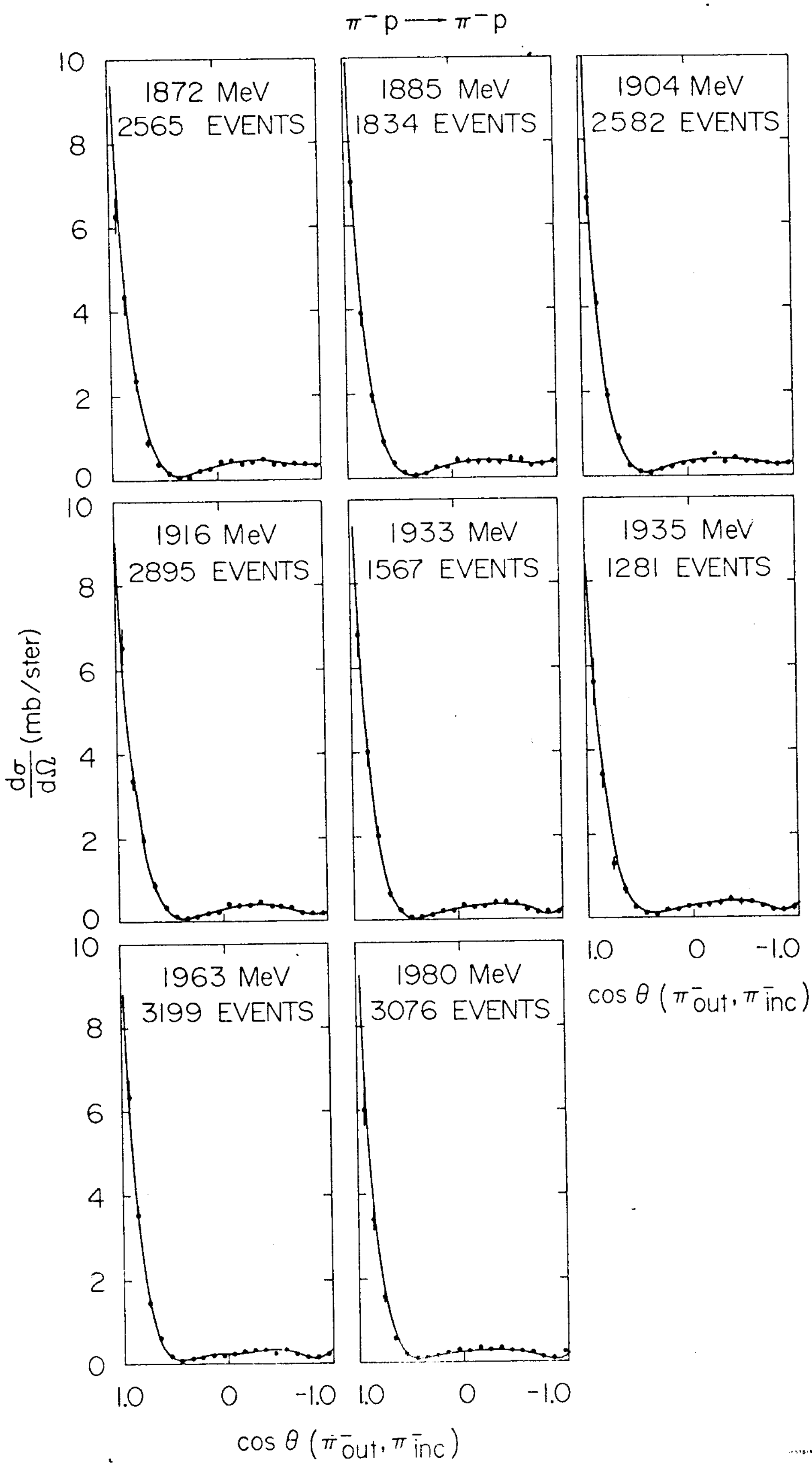

$\pi^- p \longrightarrow \pi^- p$
1872 MeV
2565 EVENTS
1885 MeV
1834 EVENTS
1904 MeV
2582 EVENTS
1916 MeV
2895 EVENTS
1933 MeV
1567 EVENTS
1935 MeV
1281 EVENTS
1963 MeV
3199 EVENTS
1980 MeV
3076 EVENTS
$\frac{d\sigma}{d\Omega}$ (mb/ster)
$\cos\theta\ (\pi^-_{out}, \pi^-_{inc})$

Fig. 11

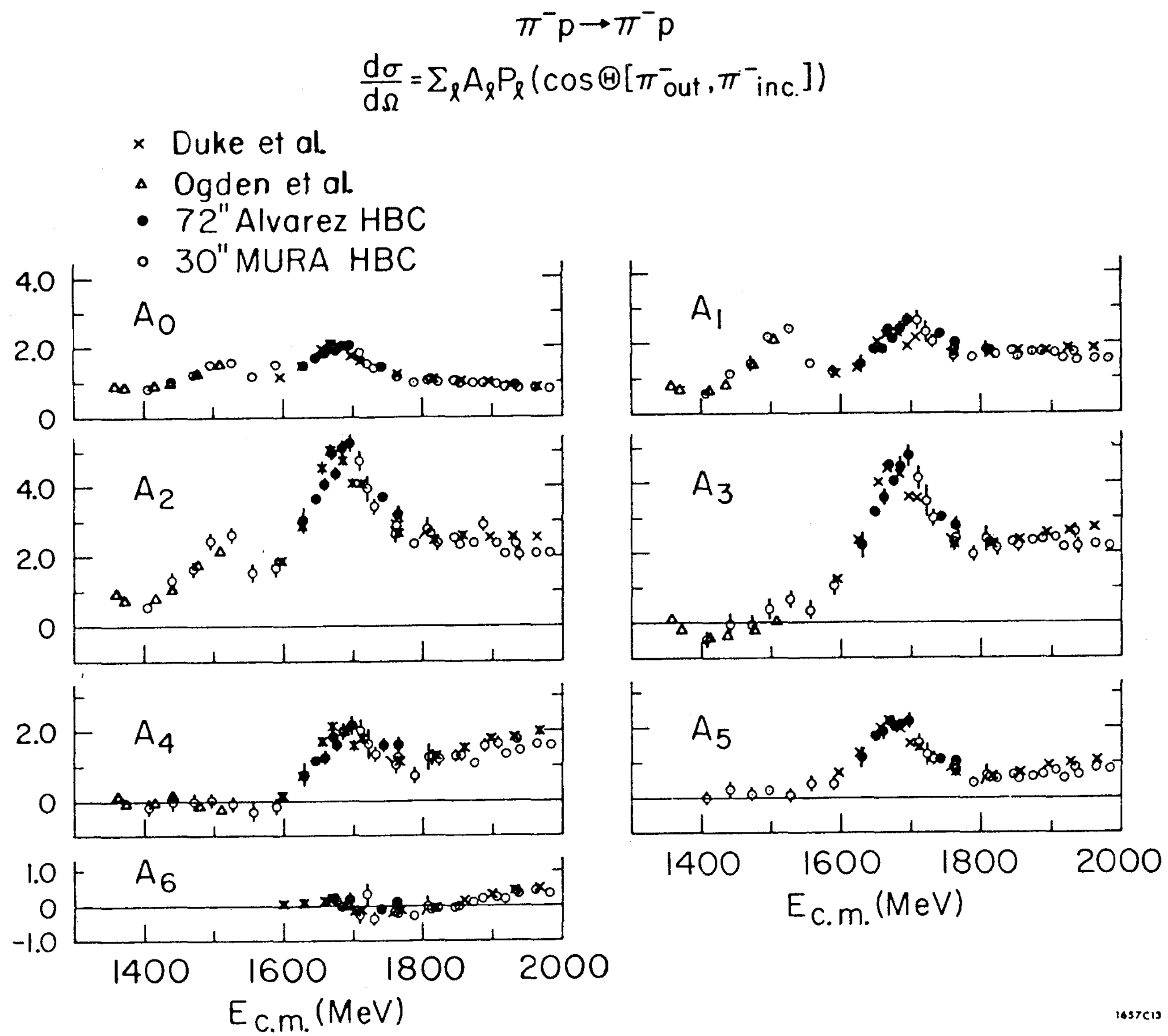

$\pi^- p \to \pi^- p$
$\frac{d\sigma}{d\Omega} = \Sigma_\ell A_\ell P_\ell (\cos\Theta[\pi^-_{out}, \pi^-_{inc.}])$
× Duke et al.
△ Ogden et al.
● 72" Alvarez HBC
○ 30" MURA HBC
A_0
A_1
A_2
A_3
A_4
A_5
A_6
4.0
2.0
0
1.0
-1.0
1400
1600
1800
2000
$E_{c.m.}$ (MeV)
1657C13

Fig. 12

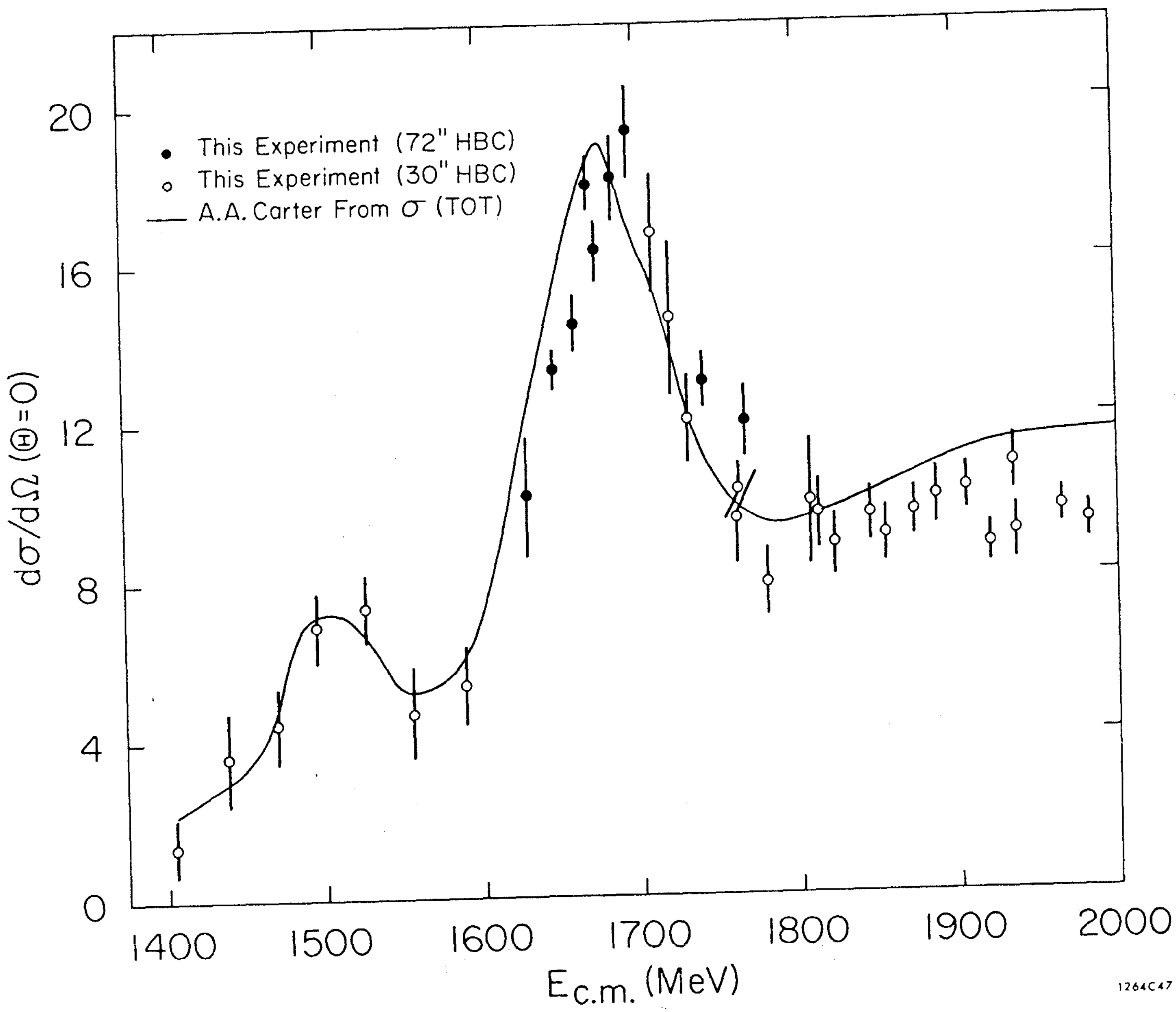

20
16
12
8
4
0
This Experiment (72" HBC)
This Experiment (30" HBC)
A.A. Carter From σ (TOT)
dσ/dΩ (Θ=0)
1400
1500
1600
1700
1800
1900
2000
Ec.m. (MeV)
1264C47

Fig. 13

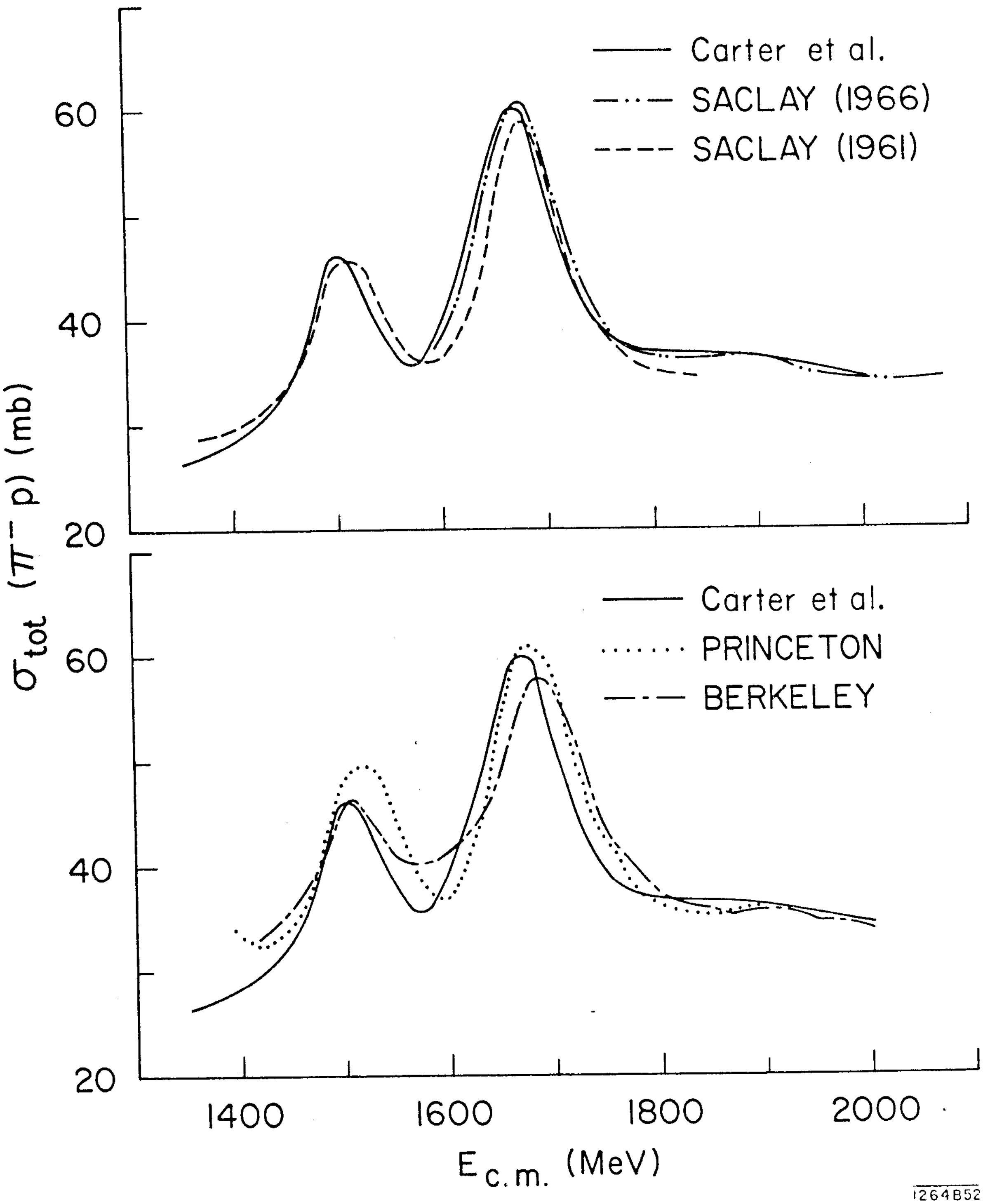
Carter et al.
SACLAY (1966)
SACLAY (1961)
60
40
20
Carter et al.
PRINCETON
BERKELEY
60
40
20
σ_{tot} (π^- p) (mb)
1400
1600
1800
2000
$E_{c.m.}$ (MeV)
1264B52

Fig. 14

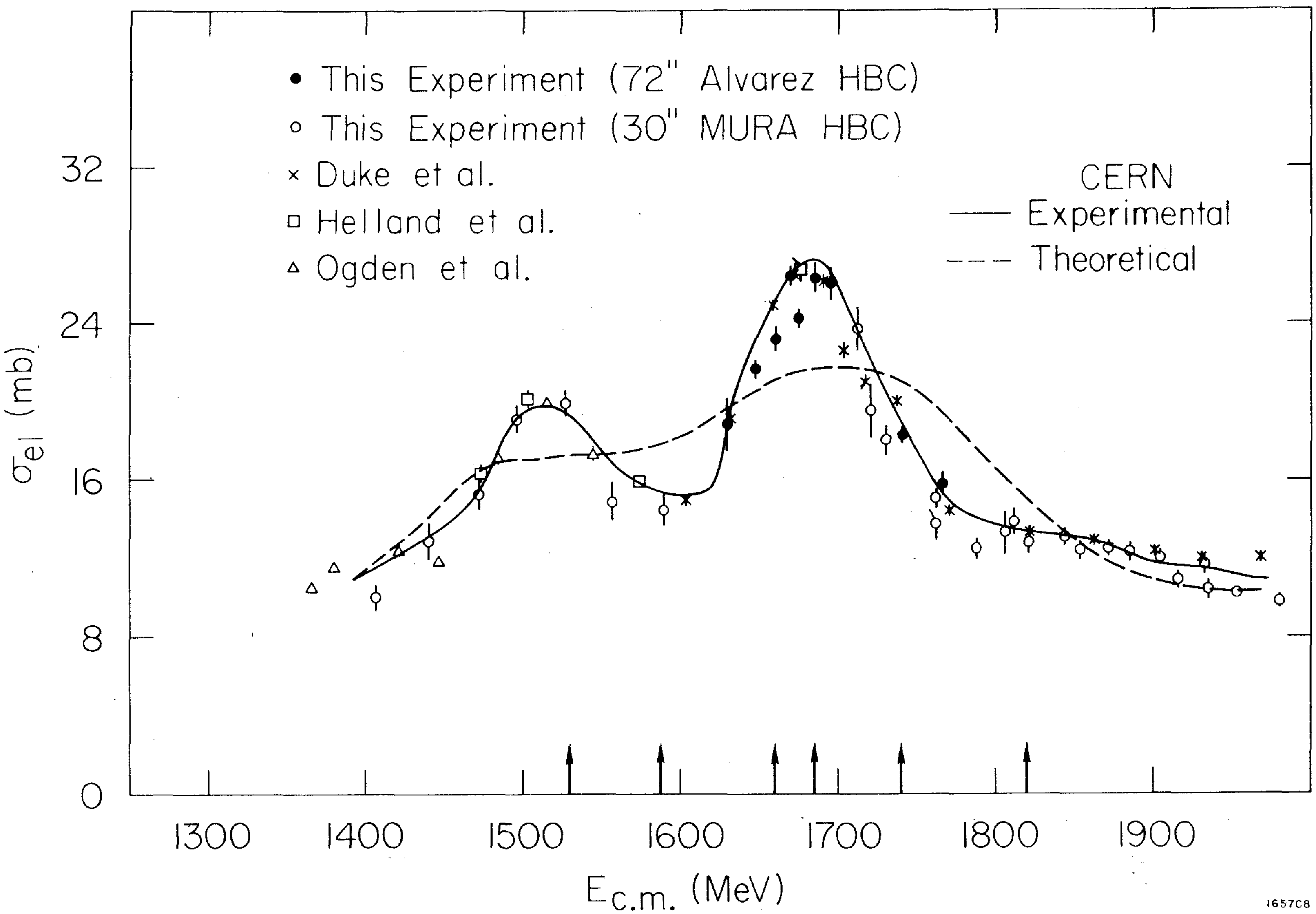

This Experiment (72" Alvarez HBC)
This Experiment (30" MURA HBC)
Duke et al.
Helland et al.
Ogden et al.
CERN
Experimental
Theoretical
32
24
16
8
0
σel (mb)
1300
1400
1500
1600
1700
1800
1900
Ec.m. (MeV)
1657C8

Fig. 15

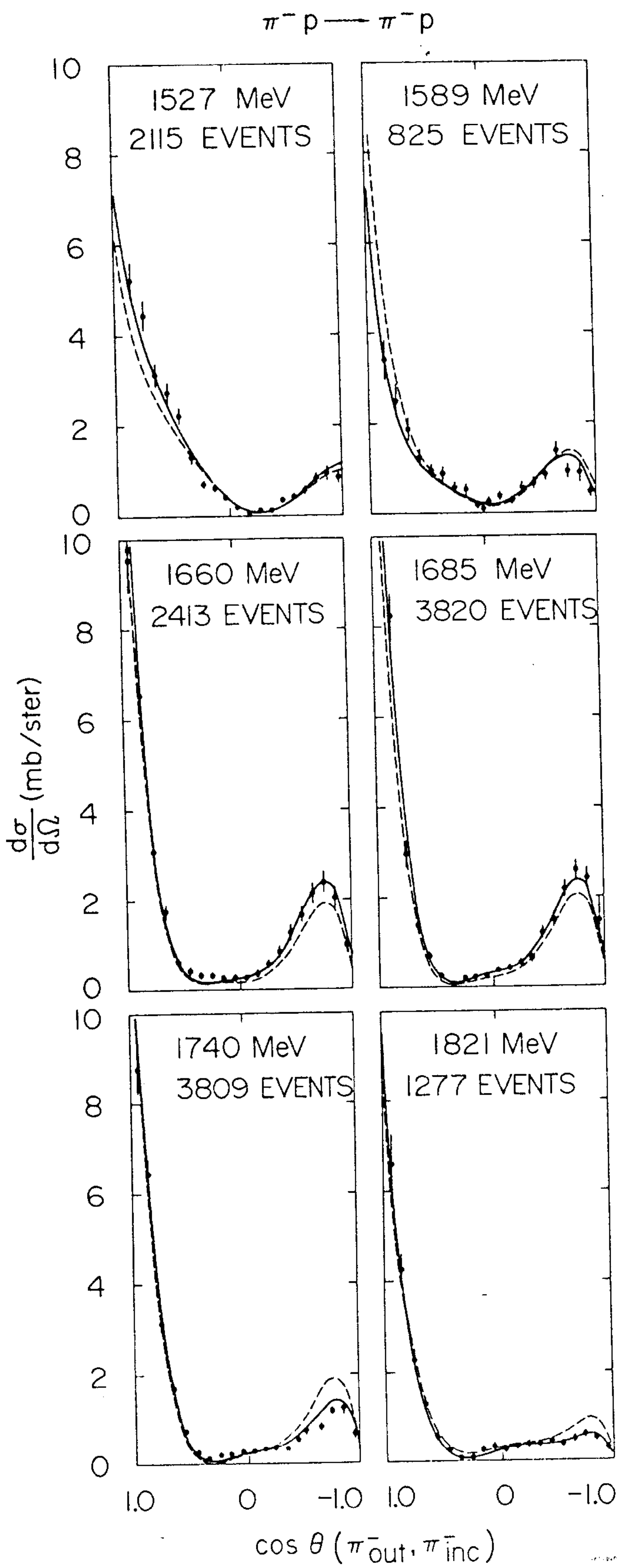

$\pi^- p \longrightarrow \pi^- p$
1527 MeV
2115 EVENTS
1589 MeV
825 EVENTS
1660 MeV
2413 EVENTS
1685 MeV
3820 EVENTS
1740 MeV
3809 EVENTS
1821 MeV
1277 EVENTS
$\frac{d\sigma}{d\Omega}$ (mb/ster)
0
2
4
6
8
10
1.0
0
-1.0
$\cos\theta\,(\pi^-_{out}, \pi^-_{inc})$

Fig. 16

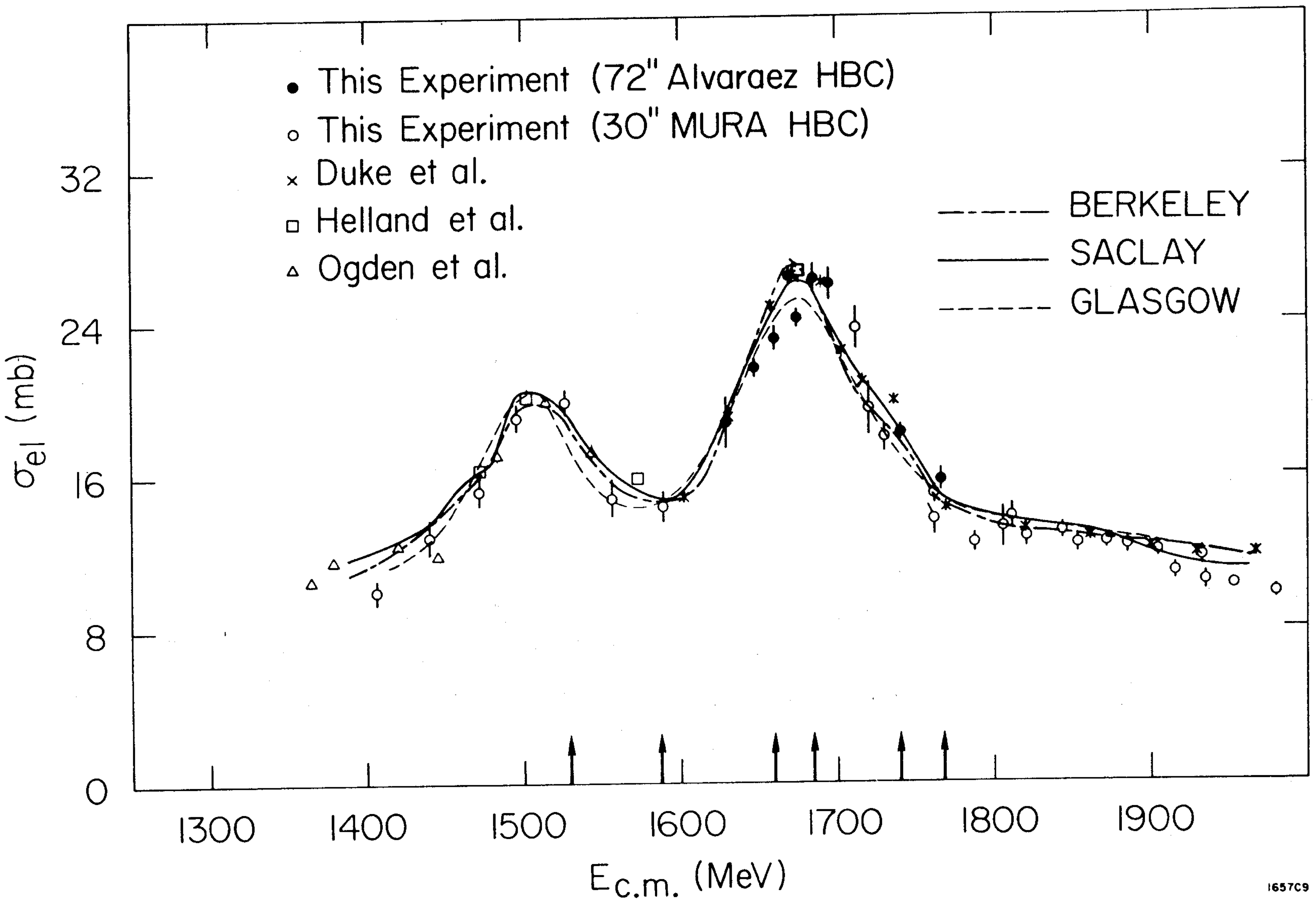

This Experiment (72" Alvaraez HBC)
This Experiment (30" MURA HBC)
Duke et al.
Helland et al.
Ogden et al.
BERKELEY
SACLAY
GLASGOW
32
24
16
8
0
σ_el (mb)
1300
1400
1500
1600
1700
1800
1900
E_c.m. (MeV)
1657C9

Fig. 17

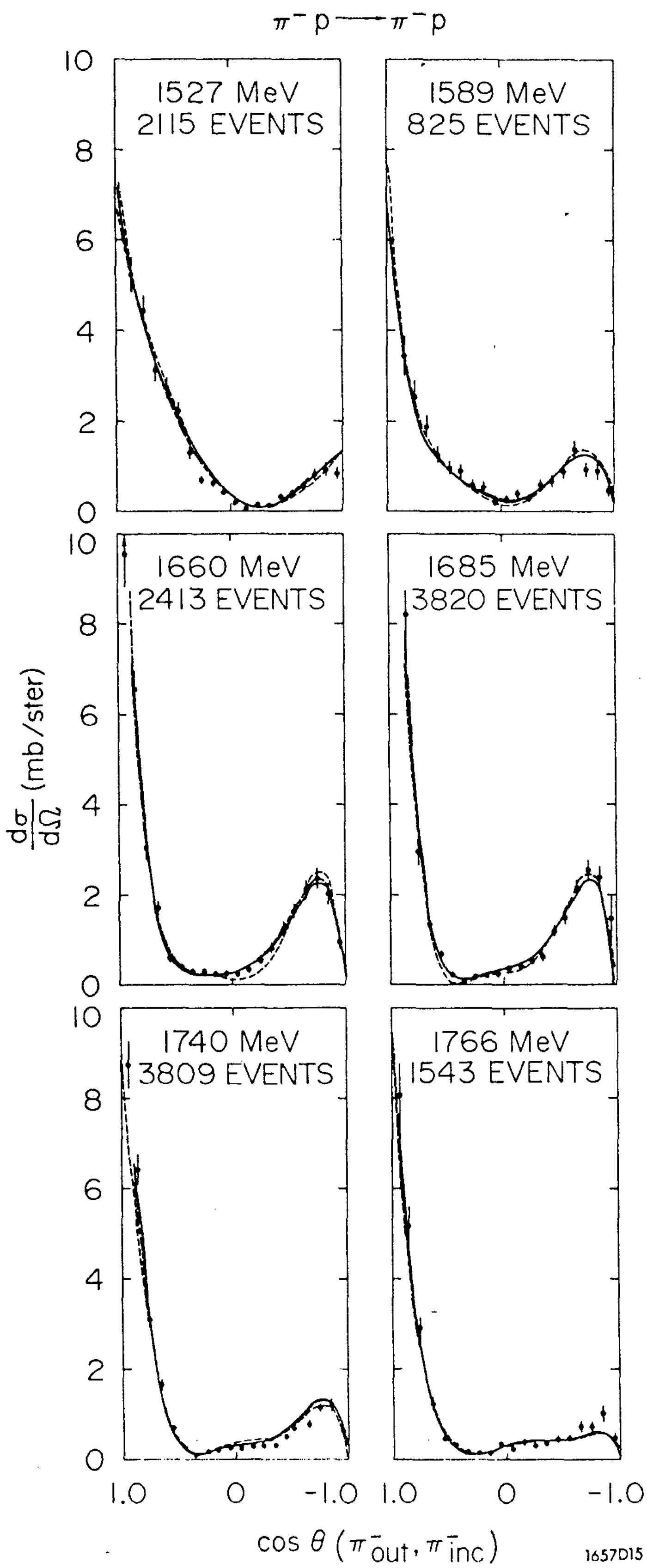

π⁻ p ⟶ π⁻ p
1527 MeV
2115 EVENTS
1589 MeV
825 EVENTS
1660 MeV
2413 EVENTS
1685 MeV
3820 EVENTS
1740 MeV
3809 EVENTS
1766 MeV
1543 EVENTS
dσ/dΩ (mb/ster)
0
2
4
6
8
10
1.0
0
-1.0
cos θ (π⁻out, π⁻inc)
1657D15

Fig. 18